OCS Study
MMS 2003-054

A Methodology for Investigation of Natural Hydrocarbon Gas Seepage in the Northern Santa Barbara Channel

Final Technical Summary

Final Study Report

U.S. Department of the Interior
Minerals Management Service
Pacific OCS Region

OCS Study
MMS 2003-054

A Methodology for Investigation of Natural Hydrocarbon Gas Seepage in the Northern Santa Barbara Channel

Final Technical Summary

Final Study Report

Authors

Bruce P. Luyendyk
Libe Washburn
Sanjoy Banerjee
Jordan F. Clark
Principal Investigators
and
Derek C. Quigley

Prepared under MMS Cooperative Agreement No. 14-35-0001-30758
by
Coastal Marine Institute
Marine Science Institute
University of California
Santa Barbara, CA 93106

U.S. Department of the Interior
Minerals Management Service
Pacific OCS Region

Camarillo
March 2003

Disclaimer

This report has been reviewed by the Pacific Outer Continental Shelf Region, Minerals Management Service, U.S. Department of the Interior and approved for publication. The opinions, findings, conclusions, or recommendations in this report are those of the authors, and do not necessarily reflect the views and policies of the Minerals Management Service. Mention of trade names or commercial products does not constitute an endorsement or recommendation for use. This report has not been edited for conformity with Minerals Management Service editorial standards.

Availability of Report

Extra copies of the report may be obtained from:

U.S. Dept. of the Interior
Minerals Management Service
Pacific OCS Region
770 Paseo Camarillo
Camarillo, CA 93010
Phone: 805-389-7621

A PDF file of this report is available at:
http://www.coastalresearchcenter.ucsb.edu/CMI/

Suggested Citation

The suggested citation for this report is:

Luyendyk, Bruce P., Washburn, Libe, Banerjee, Sanjoy, Clark, Jordan F., and Derek C. Quigley. A Methodology for Investigation of Natural Hydrocarbon Gas Seepage in the Northern Santa Barbara Channel. MMS OCS Study 2003-054. Coastal Research Center, Marine Science Institute, University of California, Santa Barbara, California. MMS Cooperative Agreement Number 14-35-0001-30758. 66 pages.

Table of Contents

List of Tables

List of Figures

FINAL TECHNICAL SUMMARY

STUDY TITLE: A Methodology for Investigation of Natural Hydrocarbon Gas Seepage in the Northern Santa Barbara Channel

REPORT TITLE: A Methodology for Investigation of Natural Hydrocarbon Gas Seepage in the Northern Santa Barbara Channel

CONTRACT NUMBER: 14-35-0001-30758

SPONSORING OCS REGION: Pacific

APPLICABLE PLANNING AREA(S): Southern and Central California

FISCAL YEAR(S) OF PROJECT FUNDING: FY 96

COMPLETION DATE OF REPORT: October, 1997

COSTS: FY 96 - $88,607

CUMULATIVE PROJECT COST: $88, 607

PROJECT MANAGERS: Bruce P. Luyendyk[1], Libe Washburn[2], Sanjoy Banerjee[3], Jordan F. Clark[4]

AFFILIATION: [1]Director, Institute for Crustal Studies, UCSB, and Professor, Geological Sciences; [2]Associate Professor, Geography, UCSB; [3]Professor, Chemical and Nuclear Engineering, UCSB; [4]Assistant Professor, Geological Sciences, UCSB

ADDRESS: University of California, Santa Barbara, CA 93106

PRINCIPAL INVESTIGATORS: Bruce P. Luyendyk, Libe Washburn, and Sanjoy Banerjee

KEY WORDS: Santa Barbara Channel; hydrocarbons; marine seeps; methane, smog, air pollution

BACKGROUND: The largest marine hydrocarbon seeps in the United States are located near Coal Oil Point in the Santa Barbara Channel (Figures 1 and 2). This investigation developed methods to quantify natural hydrocarbon seepage rates using geophysical and geochemical data. The La Goleta seep field in the Coal Oil Point area was selected as the test area because of its extreme activity. Methods to determine the amount of hydrocarbon gas being released to the atmosphere were investigated. First, the release rate can be estimated by analyzing high-resolution sonar data, because the amount of acoustic

backscatter from the gas bubbles in the water column is proportional to the amount of gas rising through the water column. Secondly, the dissolved concentrations of hydrocarbons in the ocean are proportional to the natural hydrocarbon seepage rate. Hence, their inventories in the water column can used as a method of quantifying natural hydrocarbon gas seepage rates.

OBJECTIVES: Our project objectives included developing methods to quantify the amount of hydrocarbon emissions resulting from natural gas seepage in the northern Santa Barbara Channel in 1994-1996 and establishing a baseline for future comparisons. This research would improve the air pollution emission inventory of the Santa Barbara and Ventura County Air Pollution Control Districts. In particular, it would help to quantify the amount of reactive organic gases contributed to the atmosphere by the natural seeps, and would allow documentation of future changes in the natural seepage rates.

There are five major concerns about marine seeps as natural systems, and we addressed some aspects of these in this project:
(1) What are the seeps emitting (and which seeps are emitting what)?
(2) What is the spatial distribution of oil and gas seeps in the Santa Barbara Channel?
(3) What is the natural temporal variation in seep distribution?
(4) What is the natural total emission rate, and what is its variation?
(5) What is the ultimate fate of seep emissions?

DESCRIPTION:

Specific Approach

Our research analyzed geophysical, oceanographic and geochemical data to map seeps and estimate seepage rates in the northern Santa Barbara Channel. The approach included mapping and characterizing seep areas by acoustic methods, building a scalar turbulent transport model from measured hydrocarbon concentration and current velocity data, and employing geochemical tracers to quantify emission rates, gas exchange rates, and dispersion.

The area surveyed is the Coal Oil Point seep field over the South Ellwood anticline. The western end of this oil-bearing anticline was documented as an area of natural hydrocarbon seepage in the 1970's and early 1980's and has been producing oil and gas from offshore platform Holly for nearly three decades.

The hydrocarbon seepage rises though the water column from sea floor vents above sub-sea floor hydrocarbon accumulations. Free hydrocarbon gases (bubbles), can be imaged by acoustical methods. Dissolved hydrocarbon gases are eventually liberated to the atmosphere down current from the seeps. Geochemical and oceanographic sampling and modeling are required to calculate the total hydrocarbon input to the air from this dissolved component.

Acoustic surveys

Geophysical systems used include 50 kHz, 12 kHz and 3.5 kHz echo sounding sonars to image seep bubble trains in the water column, 3.5 kHz, Uniboom, and one kilo Joule sparker seismic reflection equipment to image the sub bottom, and 325 kHz side scan sonar to map structure on the sea floor. Emission volumes for individual seeps were quantified from calibrated sonar data. A weighted hose delivered compressed air at a controlled rate from a survey ship to the sea floor. Discharge generated by this was imaged by the 3.5 and 12 kHz systems.

Side-scan sonar and sub bottom reflection systems were used to map the sea floor geology at the location of the seep vents to determine what is controlling the location of the seeps.

Dissolved hydrocarbon plume measurement and modeling

Oceanographic observations focused on the spatial structure of the dissolved hydrocarbon plume and the ambient ocean conditions which affect its dispersal. To understand the spatial structure of the plume, a ship-board gas chromatograph, configured as a "sniffer", was operated to determine the concentration and composition of hydrocarbons over the seep field. A submerged hose pulled sea water onto the research vessel where it was analyzed continuously (one complete analysis every 10 minutes) as the survey progressed. The "sniffer" data was acquired both near the sea floor and in the overlying water column. Several vertical sniffer profiles were made to resolve the vertical extent of the hydrocarbon plume.

The primary physical oceanographic measurements included vertical profiles and two-dimensional sections of water properties in and around the seep field. The detailed spatial structure of the temperature, salinity, and density fields in vicinity of the seep field was observed using a "towyo" technique in which a platform carrying a second CTD was winched between the surface and the bottom as the research vessel steams at 4-6 kts.
Time series of current velocity near the seeps was obtained from vector-measuring current meters located off the coast of Goleta, CA.

Computer modeling of dissolved hydrocarbon transport

The dynamics of the hydrocarbon plume and seepage rates from the sea floor can be inferred from sniffer data by building a scalar turbulent transport model for the area around the seeps. Using the dissolved hydrocarbon concentrations, gas solubilities, and ocean conditions (current velocity, sea water temperature, salinity, and density) as input parameters, a dissolved hydrocarbon concentration scalar field can be calculated (e.g., Radlinski and Leyk, 1995).

Tracer Release Experiments

Tracer gas release experiments were used to help calibrate both the turbulent transport model and the geophysical techniques used for determining the amount of hydrocarbon gas that is released into the atmosphere across the air-ocean interface. The dual tracer or ^{3}He - SF_6 method, has been developed which can quantify gas transfers velocities over periods of days in coastal areas (Watson et al., 1991; Wanninkhof et al., 1993; Clark et al. 1994).

Offshore Surveys

This MMS project was conducted in conjunction with three related projects funded by the University of California Energy Institute (UCEI) and awarded to Luyendyk, Washburn, and Trial. This agency, along with Mobil Corp., supported a total of six surveys prior to start of MMS funding. These surveys employed 50 kHz and 3.5 kHz sonars, and included sniffer experiments.

During the second week of August, 1996 we conducted a survey with MMS funding that included 2 days of 3.5 kHz sonar profiling along with 3 days of oceanographic sampling. We had two objectives: 1) to track dissolved hydrocarbons emitted from the seeps; and 2), repeat sonar measurements of seep intensity to study time-variations in seepage. An on-bottom SF6 tracer source was lowered to the sea floor in the seep field at the start of the survey. An acoustic Doppler current profiler was also installed on the seafloor to measure currents during the survey. The emission of the SF6 tracer and ambient hydrocarbon concentrations were measured and mapped with an on-board Gas Chromatograph and tracked for 3 days. Vertical sections of Conductivity-Temperature-Depth were obtained at the end of the tracking plume period. The sonar survey duplicated tracks we made on earlier surveys in 1995.

A sonar experiment was conducted in November to calibrate the 3.5 kHz system utilized for imaging gas seep bubble plumes. We sought to establish an empirical relation for a variety of bubble sizes and gas flux from an artificial source and the amplitude of the sonar return. The experiment was undertaken off of San Pedro, California at 120 foot water depth. A bubble release device was suspended 5 feet above the seafloor and the bubble size and flow rate were varied. Repeated passes over the bubble release device were made with the 3.5 kHz sonar towfish. Data were collected using an analog thermal recorder and also digitally at 10 kHz.

Volume flux emission estimates from the calibrated 3.5 kHz data were compared to estimates based on a previous calibration of 50 kHz sonar data and determined that the total emissions estimated using the two different sonar systems are similar in magnitude. We arranged for a side scan sonar survey of the study area that will yield a high resolution map-view image of the sea floor. The side scan sonar map will help us understand the structural geological characteristics of the hydrocarbon seeps field.

Our final efforts involve finishing the side scan mapping, refining the relation between signal strength and gas flux, mapping the detailed seafloor geology, and preparing two manuscripts for publication; one on a quantitative estimate of gas discharge form this seep field, and a second on the dissolved gas content of the ocean waters around the seep field.

SYNOPSIS OF MAJOR FINDINGS or SIGNIFICANT CONCLUSIONS: Our analysis of the calibrated sonar data suggest a Coal Oil Point seep field flux of 1.1 x 105 m3/day for the 3.5 kHz data. Adding the contribution from the seep tents near offshore Platform Holly gives a total estimate of 1.2 x 105 m3/day. This compares favorably with the estimate from the our calibrated 50 kHz sonar data of 1.5 x 105 +/- 0.2 m3/day (5.3 x

106 ft3/day). The methane emission rate we determined is 72 +/- 11 metric tonnes/day and the non-methane hydrocarbon rate is 30 +/- 4 metric tonnes/day. Reactive organic gas (ROG) emissions from the seeps are 19 +/- 3 metric tonnes/day. Our estimated methane emission rate for the Coal Oil Point field is five times higher than previous estimates. The most intense areas of seepage correspond to structural culminations along anticlinal axes. Seep locations are mostly unchanged from those documented in 1946, 1953, and 1973. An exception is the seepage field that once existed near offshore oil Platform Holly. A 50% reduction in seepage within a one kilometer radius around this offshore platform is correlated with reduced reservoir pressure beneath the natural seeps due to oil production. The decrease in hydrocarbon seepage rate near Platform Holly suggests that oil production here has resulted in an unexpected benefit to the marine and atmosphere environment.

The reactive organic gas emission rates from the Coal Oil Point seeps alone are a large source of hydrocarbon air pollution in Santa Barbara County (equal to the emission rate from all the vehicle traffic in the County in 1990). The ROG emission rates found in our study for Coal Oil Point seep field are three times the seep ROG emission rates estimated in the official Santa Barbara County air emission inventory (SBCAPCD, 1994). Furthermore, Fischer (1977) estimated that the Coal Oil Point seep field contains only half of the marine seeps in Santa Barbara County. The official Air Pollution Control District estimate of ROGs in Santa Barbara County is therefore too low by at least a factor of four (Saxena and Oliver, 1984). Reaching EPA air quality attainment status in Santa Barbara County may require an effective means of containing or remediating the natural seeps.

Surveys of dissolved hydrocarbons within 15 km the Coal Oil Point seep field identified a plume which extends down-current of the seeps. In most samples, ethane and propane concentrations correlated well with methane concentration. The maximum and mean methane concentrations within the plume were approximately 5200 nmol l-1 and 1300 nmol l-1, respectively. Concentration distributions were characterized by areas of high and low concentrations which did not correspond to different regions of the plume. These areas resulted from the complicated geometry of the seep field as well as the chaotic nature of mixing within the field area. Mass balance calculations indicate that approximately half of the methane (30% - 60%) dissolves during transit through the water column.

Cynar and Yayanos (1992) showed that a subsurface methane maximum occurs along a narrow density horizon throughout most of the Southern California Bight. They argued that this maximum was supported by coastal sources including natural hydrocarbon seeps. At the time of our survey, the density of the water receiving the influx of methane from the Coal Oil Point seeps was similar to the density of the water containing the subsurface methane maximum Cynar and Yayanos (1992) observed off shore. Furthermore, the total flux of methane into water column from the Coal Oil Point seeps, $2.4 \pm 0.6 \times 1010$ g yr-1, is approximately equal to the total flux of dissolved methane to the atmosphere over this broad area. These observations strongly support the inference that coastal sources maintain the excess methane observed off shore as argued by Cynar and Yayanos (1992) and Ward (1992).

We also have completed a high resolution isopach map of the Quaternary overburden in the Coal Oil Point seeps study area. We found that a great portion of the seep field is not coated by a thick layer of pelagic and terrigenous sediment, but rather by less than a meter of apparently unconsolidated overburden above siliceous shale of the Sisquoc formation. Our computer models of advection of dissolved hydrocarbons agree well with observations. These show that the modeling technique is valid and well constrained by the data we obtained. The model can therefore be used to predict the dispersion of dissolved hydrocarbons in the Channel.

STUDY RESULTS:

1. Gas volume discharge has been estimated for the Coal Oil Point seep field.
2. The concentration of dissolved hydrocarbons from the seep discharge has been mapped and quantified.
3. Seep intensity has decreased around offshore Platform Holly since 1973.

STUDY PRODUCTS:

1. Map of gas seep locations
2. Estimates of seep gas discharge
3. Map of dissolved hydrocarbon plume
4. Model of advection of dissolved hydrocarbons away from Coal Oil Point.

Publications:

Boles, J.R., Clark, J.F., Leifer, I., and L. Washburn. 2001. Temporal variation in natural methane seep rate due to tides, Coal Oil Point area, California. *J of Geophys Res-Oceans* **106**(C11): 27077-27086.

Clark, J.F., Washburn, L., Hornafius, J.S., and B.P. Luyendyk. 2000. Dissolved hydrocarbon flux from natural marine seeps to the southern California Bight. *J of Geophys Res-Oceans* **105**(C5): 11509-11522.

Hornafius, J.S., Quigley, D., and B.P. Luyendyk. 1999. The world's most spectacular marine hydrocarbon seeps (Coal Oil Point, Santa Barbara Channel, California): Quantification of emissions. *J Geophys Res-Oceans* **104**(C9): 20703-20711.

Quigley, D.C., Hornafius, J.S., Luyendyk, B.P., Francis, R.D., Clark, J., and L. Washburn. 1999. Decrease in natural marine hydrocarbon seepage near Coal Oil Point, California, associated with offshore oil production. *Geology* **27**(11): 1047-1050.

Derek C.Quigley. 1997. *Quantifying Spatial and Temporal Variations in the Distribution of Natural Marine Hydrocarbon Seeps in the Santa Barbara Channel, California*. M.S. thesis, University of California, Santa Barbara. 95 pp.

Research Presentations:

American Geophysical Union Meeting

Our research group made four presentations on our seeps project at the Fall '96 AGU meeting in San Francisco December 18 (list follows). These presentations were directly supported by the MMS project, along with additional support from the University of California.

Bartsch, E.C., Gurrola, L.D., Francis, R.D., Quigley, D.C., Hornafius, J.S., and Luyendyk, B.P., *Structural Control of the Spatial Distribution of Hydrocarbon Seeps in the Santa Barbara Channel, California*, EOS Trans. Amer. Geophys. Union, vol. 77, no. 46, F419.

Clark, J.F., Washburn, L., Hornafius, J.S., Luyendyk, B.P. and Ho, D.T., *Mixing in the Vicinity of Natural Marine Hydrocarbon Seeps, Santa Barbara Channel, CA*, EOS Trans. Amer. Geophys. Union, vol. 77, no. 46, F419.

Quigley, D.C., Hornafius, J.S., Luyendyk, B.P., Francis, R.D., and Bartsch, E.C., *Temporal Variation in the Spatial Distribution of Natural Marine Hydrocarbon Seeps in the Santa Barbara Channel, California*, EOS Trans. Amer. Geophys. Union, vol. 77, no. 46, F419.

Washburn, L., Hornafius, J.S., Luyendyk, B.P., Clark, J.F., Quigley, D.C., and Francis, R.D., *Dispersal of Hydrocarbon Gas Plumes from Seafloor Seeps in the Northern Santa Barbara Channel, CA*, EOS Trans. Amer. Geophys. Union, vol. 77, no. 46, F419.

REFERENCES:

Clark, J. F., R. Wanninkhof, P. Schlosser, and H. J. Simpson. 1994. Gas exchange rates in the tidal Hudson river using a dual tracer technique. Tellus, 46B, 274-285.

Cynar, F. J. and Yayanos, A. A. (1992) The distribution of methane in the upper waters of the Southern California Bight: Journal of Geophysical Research, v. 97, p. 11,269-11,285.

Fischer, P. J., 1977, Natural gas and oil seeps, Santa Barbara basin, California, in California Offshore Gas, Oil, and Tar Seeps: State of California, State Lands Commission staff report, p. 1-62.

Radlinski, A. P. and Leyk, Z., 1995. Formation of light-hydrocarbon anomalies in oceanic waters. Geology, 23, 265-268.

Saxena, P., and Oliver, W. R., 1984, Estimation of reactive organic gas emissions from offshore oil and gas seeps in the Santa Barbara Channel: Systems Applications, Inc., report SYSAPP-84/197 prepared for the Environmental Protection Agency, Region IX, San Francisco, California, 25 p.

Santa Barbara Air Pollution Control District, 1994, The 1994 Clean Air Plan, Appendix D., Table 3.2, Santa Barbara, CA.

Wanninkhof, R, W. Asher, R. Weppernig, H. Chen, P. Schlosser, C. Langdon, and R. Sambrotto. 1993. Gas transfer experiment on Georges Bank using two volatile deliberate tracers. J. Geophys. Res. 98, 20,237-20,248.

Ward, B. B. (1992) The subsurface methane maximum in the California Bight. Continental Shelf Research, 12, 735-752.

Watson, A. J., R. C. Upstill-Goddard, and P. S. Liss. 1991. Air-sea exchange in rough and stormy sea measured by a dual tracer technique. Nature, 349, 145-147.

FINAL STUDY REPORT

UNIVERSITY OF CALIFORNIA
Santa Barbara

Quantifying Spatial and Temporal Variations in the Distribution of Natural Marine Hydrocarbon Seeps in the Santa Barbara Channel, California

Thesis submitted in partial satisfaction of the requirements for the degree of

Master of Science
in
Geophysics

by
Derek C. Quigley

Committee in charge:
Professor Bruce Luyendyk, chairperson
Professor Jim Boles
Professor Jordan Clark

September 1997

ABSTRACT

Quantifying Spatial and Temporal Variations in the Distribution of Natural Marine Hydrocarbon Seeps in the Santa Barbara Channel, California

Derek C. Quigley

Prolific natural hydrocarbon seepage offshore of Coal Oil Point in the Santa Barbara Channel, California contributes significant quantities of gaseous and liquid hydrocarbons to the local environment, and may also represent an important process at the global scale. Insight into rates of seepage improves the understanding of local pollution from seeps and global seepage potential. Constraining the volume of fluid migration in the crust associated with seepage is also relevant since such fluid movement can mark diagenetic processes and affect parameters of structural stability causing earthquake swarms. The distribution of gaseous seepage offshore of Coal Oil Point was mapped using 3.5 and 50 kHz sonar by imaging rising seep gas bubbles which act as acoustic scattering targets within the water column. Examination of a series of mapped seep distributions reveals the following: (1) spatial location of seeps is principally controlled by structural features of the offshore geology, aligning with the east-west structural trends of anticline axes; (2) intensity of seepage emission correlates with structural relief and perhaps cross-cutting by faults; (3) both spatial distribution of seepage and volume emission rates vary over time; (4) drawing down of reservoir hydrocarbons and the reduction in reservoir pressure associated with offshore oil production is one contributing factor decreasing the extent of seepage and seep emission volumes; (5) areal extent of seep distribution within 13 km^2 of platform Holly decreased from 0.9 to 0.4 km^2 and volumetric emission declined on the order of 50,000 m^3/day between 1973 and 1995; (6) a current estimate of volumetric flux from seeps for the entire Coal Oil Point offshore area suggests emission is on the order of 1-2x10^5 m^3 of gas per day and 20,000-30,000 liters of oil.

1.0 INTRODUCTION

This thesis is a study of natural marine hydrocarbon seepage offshore of Coal Oil Point in the Santa Barbara Channel, California. The object of the study is to quantify seep emissions and estimate the flux of hydrocarbons from the seeps. Natural submarine hydrocarbon seepage may contribute considerably to global cycling of carbon within the marine environment and is certainly a substantial source of pollution within Santa Barbara County. Therefore, this issue is an important topic of scientific inquiry.

At the local level, the prolific natural oil and gas seepage offshore Coal Oil Point represents a significant source of pollution. Non-methane hydrocarbons which comprise a portion of the gaseous seepage (Table 1) constitute reactive organic gases (ROG's) which are introduced to the Santa Barbara Air Basin. These gases are precursors to smog forming ozone, and represent a health risk to Southern California residents. Saxena and Oliver [1984] estimated natural hydrocarbon seeps in the Santa Barbara Channel produced 18 to 152 tons of ROG's per day. By comparison, all the on-road vehicle traffic in Santa Barbara County accounted for only 17 tons per day of ROG's in 1990 [Santa Barbara Air Pollution Control District, 1994]. Canister hydrocarbon data collected by Killus and Moore [1991] around the South Central Coast air basin suggest that geogenic sources of hydrocarbon trace gases (i.e.-natural gas seeps) dominate over anthropogenic sources (automobile emissions) in the local atmosphere. In fact, chemical analyses of these air grab samples indicated 86% of the non-methane hydrocarbons in the samples originated from natural oil and gas seeps.

Table 1: ANALYSES OF NATURAL SEEP GASES COLLECTED NEAR THE ARCO/MOBIL SEEP TENTS

Sample date	6/8/73	6/27/73	8/3/73	6/15/73	9/13/94
Sample Description	Monterey Produced Gas	Seep Gas from Ocean Floor*	Seep Gas from Ocean Floor**	Seep Gas from Ocean Surface	Seep Gas from Seep Tents
Composition	Mole%	Mole%	Mole%	Mole%	Mole%
Nitrogen	0.24	0.23	1.09	0.00	0.235
Carbon Dioxide	9.39	11.50	9.66	0.00	0.916
Methane	68.738	78.635	80.250	89.370	89.051
Ethane	8.749	5.566	4.919	4.330	5.287
Propane	6.636	2.703	2.713	3.650	2.911
Iso-Butane	0.966	0.300	0.302	0.720	0.365
N-Butane	2.178	0.678	0.603	0.980	0.699
Iso-Pentane	0.612	0.131	0.128	0.220	0.204
N-Pentane	0.553	0.090	0.098	0.160	0.204
Hexane+	0.758	0.167	0.237	0.570	0.081
Hydrogen Sulfide	1.180	0.00	0.00	0.00	0.002
Specific Gravity	0.862	0.747	0.731	0.658	0.6448
BTU/SCF	1222	1019	1026	1174	1018

*Sampled by Atlantic Richfield
**Sampled by the State Lands Commission

In addition, the methane in the seep gas (approximately 90% by volume) is of interest because it is a greenhouse gas. After carbon dioxide, methane is the most significant contributor to radiative forcing [Shine *et al.*, 1990]. Concentration of methane in the atmosphere is currently increasing at about 0.9% per year [Watson *et al.*, 1990]. Given the speculation that increased concentrations of atmospheric methane released from destabilized methane gas hydrates may have contributed to global climate change in the past [MacDonald, 1990; Nisbet, 1990; Kvenholden, 1993], an accurate understanding of the sources and sinks of methane is an important scientific issue [Cicerone and Oremland, 1988].

Venting of methane from submarine seeps has been suggested as a significant, and previously overlooked, source of methane in the oceans [Hovland *et al.*, 1993]. Dissolved methane concentrations in the upper oceans exceed expected levels based on atmospheric equilibrium [Cynar and Yayanos, 1992]. Since submarine methane seepage is hypothesized to effect ocean chemistry {Dando and Hovland, 1992], natural seeps may be responsible for this discrepancy. In addition, methane leaking from the sub-seabed is depleted in ^{14}C, which could account for the

shortfall in fossil methane calculated for current atmospheric methane budgets [Lacroix, 1993; Hovland *et al*., 1993].

In addition to the flux of methane and other gaseous hydrocarbons from the seeps offshore Coal Oil Point, seepage of liquid petroleum can lead to surface oil slicks and tar balls in the vicinity. Liquid petroleum (oil and tar) has a greater potential as a marine pollutant due to its long term presence as opposed to gaseous components which are either lost to the atmosphere or quickly assimilated. Previous authors [Kvenholden and Harbaugh, 1983; Landes, 1973; Wilson *et al*., 1974] have addressed the issue of liquid petroleum seepage as a significant source of natural pollution within the marine environment.

Volatile gases evaporating from the surface slicks off Coal Oil Point contribute additional ROG's to the atmosphere. The residual tar is found in abundance on Santa Barbara Channel beaches [Welday, 1977]. Hartman and Hammond [1981] claimed based on isotope analysis that nearly all of the tar found along the Santa Barbara coastline and 55% of the tar collected in Santa Monica Bay, 150 km away, had originated from seeps at Coal Oil Point. Emission of oil and tar from the Coal Oil Point seeps is therefore another topic of concern.

In addition to estimating the volume of seep emissions in the Coal Oil Point area, a second important goal of this thesis project is to address the issue of time variation in seep emission rates. Previous authors have proposed rates of hydrocarbon leakage vary over time [Wilkinson, 1972; Fischer and Stevenson, 1973; Fischer, 1977; Kvenholden and Harbaugh, 1983; Clarke and Cleverly, 1991; Hovland *et al*., 1993]. It is important to understand the magnitudes of such fluctuations and the mechanisms responsible if one is interested in addressing processes which are changing in time such as the increasing concentration of atmospheric methane alluded to previously.

The reasons outlined above demonstrate the importance of understanding emission rates from the natural marine hydrocarbon seeps at Coal Oil Point. These seeps are a significant local source of marine pollution (oil and tar) and air pollution (ROG's) in Santa Barbara. Submarine seepage may also be important globally as a natural pollution source, affecting ocean chemistry and atmospheric quantities of methane. For these reasons, it is important to quantify the emission volumes from these natural seeps and examine the time variation in seep emission rates.

2.0 ENVIRONMENT OF NATURAL HYDROCARBON SEEPS

Natural hydrocarbon seeps are a well known occurrence throughout the world and historical references to seepage date back to earliest recorded history. Asphalt from seeps in the Middle East has been used as a building material since 3,000 BC, and burning gas seeps in the Baku region were known from several centuries before Christ [Hunt, 1979]. Documented written records of seeps include biblical references, and the works of Herodotus and Marco Polo [Wilson *et al*., 1974]. Historically, natural hydrocarbon seeps have provided a useful tool for petroleum exploration [Link, 1952; Hunt, 1979; Tedesco, 1995].

Link [1952] states that the significance of seeps from an exploration standpoint is that they prove the presence of source hydrocarbons and suitable structural traps for their accumulation. The presence of hydrocarbons is necessary for hydrocarbon seepage, and this requires a sufficient thickness of sedimentary rock and source rocks for hydrocarbon generation within the sedimentary section. Therefore, hydrocarbon seeps are commonly found throughout the world in sedimentary basins containing oil reserves.

Structures for hydrocarbon accumulation and structural pathways for fluid migration are also important factors contributing to the presence of seepage. Conduits along which fluid movement could occur include layer contacts, interbedded lenses, or faults, although in the absence of fluid pathways in the subsurface the hydrocarbons may move as an amorphous plume [Machel and Burton, 1991].

Hunt [19791 notes that seeps throughout the world are most numerous at the margins of basins in sediments that have been faulted, folded, or eroded, thus creating structures, pathways, and exposures conducive to hydrocarbon accumulation, migration, and subsequent leakage. Link [1952] categorized the types of structures associated with instances of hydrocarbon seepage as follows: (1) seeps emerging from the ends of homoclinal beds where the beds are exposed at the surface, (2) seeps associated with beds and formations in which the oil was formed, (3) seeps from large oil accumulations bared by erosion or ruptured by faulting or folding, (4) seeps at the outcrops of unconformities, and (5) seeps associated with intrusions such as mud volcanoes, igneous intrusions, and piercement salt domes.

Conduits for hydrocarbon seepage are frequently provided by fault induced fracture pathways for fluid movement. Hunt [1979] states: “Fissuring and fracturing associated with faulting induces secondary permeability and porosity, which favor vertical fluid migration”. Faults may also create impermeable seals depending on the nature of faulting and the lithologies of the superposed units. Hunt [1979] notes that tensional fractures in hard, brittle rocks favor vertical migration whereas faults in clay or shale sections tend to smear clay gouge on the fault plane creating a seal. Seals at faults may also result in otherwise permeable units due to hydrodynamic effects, or capillary phenomena [Eremenko and Michailov, 1974]. Nevertheless, numerous examples [Link, 1952] illustrate that faulting often results in important migrational pathways for seepage.

Given the role of faulting in creating seepage pathways, seismic activity is an important factor in the occurrence of seepage. In assessing the seepage potential of the world’s continental margins Wilson *et al*. [1974] defined the highest seepage potential as the margins of sedimentary basins located along plate boundaries where earthquake activity was high. In contrast, tectonically stable areas such as the Gulf of Mexico exhibit comparatively little seepage despite the presence of large oil reserves [Hunt, 1979]. Seismic activity ostensibly augments the available network of fracture conduits which serve as fluid migration pathways, thus enhancing seepage.

Fault fracture meshes form important conduits for large volume fluid flow and can also generate earthquake swarms [Sibson, 1996], which are known to occur in the Santa Barbara Channel [Sylvester *et al*., 1970; Sibson, 1996] although in general earthquake swarms are comparatively

rare within settings of active compressional tectonics. This study of hydrocarbon seepage at Coal Oil Point could conceivably be important for the understanding of earthquake hazards in the Santa Barbara area.

The presence of pressurized fluid in reservoirs has previously been linked with seismic activity and earthquake swarms [Healy *et al*., 1968; Gibbs *et al*., 1973]. Earthquake swarms may result from heterogeneity in the distribution of stress concentrations in the crust [Hill, 1977] which are affected by fluid distribution [Hubbert and Rubey, 1959]. The Monterey formation, which is the origin of the oil and gas leaking at the Coal Oil Point seeps [Reed and Kaplan, 1977; Hartman and Hammond, 1981], is an example of interlayered beds of strong competence contrast leading to well developed Hill-type meshes [Sibson, 1996]. These are structures conducive to both fluid flow (seepage) and earthquake swarm activity.

3.0 MECHANISMS OF HYDROCARBON MIGRATION AND SEEPAGE

Seepage in the literature is divided into macroseepage and microseepage. Macroseepage refers to a macroeffusion of hydrocarbons in large quantities such as the massive outpouring or ejection of fluid in an extrusive volcanic flow. Microseepage implies a less voluminous discharge not visible to the naked eye but which can be sensed using enhanced analytical techniques. Sensing of such surface geochemical anomalies has been used as an exploration tool for identifying new hydrocarbon reservoirs. Clarke and Cleverly [1991] note that conditions for subsurface movement of oil and gas preclude the flow of trace quantities, so microseepage may actually indicate the presence of hydrocarbon residues in soils as a product of near-surface seep dispersal.

The Coal Oil Point seeps clearly qualify as an instance of macroseepage. This can involve leaking of hydrocarbons either directly from source rocks or from reservoir beds. Possible forms of macroseepage summarized by Tedesco [1995] include: (1) mass migration through open faults and fractures, (2) megaventing along migrational pathways, (3) flowing from overpressurized and breached reservoirs via faults, (4) expelling from currently generating hydrocarbon source rocks, and (5) occasional venting from basement penetrating faults. The migration of hydrocarbons along these subsurface pathways which ultimately leak to the surface leads to seepage.

Traditionally hydrocarbon migration has been divided into primary and secondary migration. Hunt [1979] defines these as follows: primary migration is the movement of oil and gas out of source rocks into permeable reservoir rocks while secondary migration is the movement of fluids within the permeable rocks of the reservoir which eventually leads to segregation and accumulation of oil and gas. The transport mechanisms responsible for hydrocarbon movement tend to differ depending on whether one refers to primary or secondary migration, mostly due to the difference in permeability between source and reservoir units. Factors other than permeability may also come into play, including the quantity of organic matter present and the geochemistry of the transported hydrocarbons. Many details regarding hydrocarbon migration are still the topic of debate, despite having received considerable attention in the literature [Roberts and Cordell, 1980; Doligez, 1987; England and Fleet, 1991].

Seepage in some senses falls outside the traditional definitions of primary or secondary migration as presented by Hunt. It refers to post-accumulation migration and leakage of hydrocarbons at the surface [Clarke and Cleverly, 1991]. In general, the mechanisms of secondary migration would be more applicable to seepage in that leaking typically occurs within the more permeable reservoir units, although seepage can also occur directly from source rocks [Link, 1952]. For our purposes, we are most concerned with the mechanisms of hydrocarbon migration applicable within the context of seepage.

Primary migration probably occurs as petroleum-phase expulsion of distinct oil globules from source rocks [Tissot, 1987], and may occur along a kerogen network of organic matter [McAuliffe, 1979]. The role of water may be important for secondary migration, hydraulically driving separate phase hydrocarbon transport [England and Fleet, 1991]. It is unlikely that hydrocarbon migration involves transport in either aqueous or colloidal solution, but rather the hydrocarbons move as a distinct phase from the water which saturates the carrier beds. Migration in aqueous solution is unlikely due to the extreme insolubility of petroleum in water. Although this solubility increases with temperature and pressure [Price, 1976; 1979], it is also dependent on hydrocarbon species, and no fractionation of known petroleum accumulations based on solubility has been observed. Similarly, hydrocarbon migration in a colloidal (micellar) solution is unlikely since there is no evidence that petroleum accumulations fractionate based on their ability to form micelles.

The forces driving hydrocarbon migration result from disequilibrium in the subsurface and transport hydrocarbons in the direction of decreasing free energy [Hunt, 1979]. Flow regimes include gravity-, pressure-, and density-driven transport [Tedesco, 1995]. Gravity tends to drive fluids downward towards the lowest potential energy. More often, however, pressure is dominant and directed upward [Hunt, 1979], counteracting gravity. The pressure arises from compactional disequilibrium, thermal expansion, and generation of gas [Tedesco, 1995].

Pressure is probably the dominant driving force for primary hydrocarbon migration [Tissot, 1987], squeezing oil from the source rocks [du Rouchet, 1981]. Buoyancy arising from density variations accompanying changes in temperature and salinity can also counteract gravity and is the likely driving mechanism for secondary migration [England and Fleet, 1991]. Capillary pressure resists buoyancy driven transport, which would oppose the expulsion of oil-phase droplets within environments of restricted permeability, leading previous authors to argue against petroleum-phase expulsion as a mechanism for primary migration [Cordell, 1972; Price, 1976; McAuliffe, 1979; Hunt, 1979].

On the other hand, separate phase flow of natural gas, consisting primarily of methane, can migrate at permeabilities which would restrict oil-phase migration. Methane could dissolve increasing amounts of heavier liquid hydrocarbons as temperature and pressure increase [Hunt, 1979], possibly allowing gas-phase migration of liquid hydrocarbons in gas solution. Disequilibrium in concentration could lead to diffusive transport of gaseous hydrocarbons which has been proposed as an effective mechanism for the movement of gas but not for oil [Leythauser *et al*., 1982]. However, the principle objection to diffusion as the primary form of hydrocarbon transport is that the rates involved are extremely slow [Hunt, 1979]. Krooss *et al*. [1992]

acknowledged that diffusive transport through water-saturated cap rock is likely to be less efficient than either free gas-phase flow or transport of dissolved gas in aqueous solution.

Buoyant transport is typically the principle driving force for vertical migration which results in surface seepage since buoyancy of the gas phase dominates the fluid potential gradients in the near subsurface driving secondary migration along postaccumulation seepage pathways [Clarke and Cleverly, 1991]. Pressure is typically dominant driving primary migration at depth [Tissot, 1987] but could also be effective in the shallow subsurface. In addition, regional gravity driven flow of meteoric recharge waters might affect migration patterns of seepage, deflecting migrating hydrocarbons from their subsurface accumulations through advection by groundwater [Machel and Burton, 1991].

4.0 TIME VARIATION IN EMISSION AND DISTRIBUTION OF SEEPAGE

Previous work has alluded to the time variation of seepage rates and seep distribution at Coal Oil Point [Allen *et al*., 1970; Wilkinson, 1972; Mikolaj and Ampaya, 1973; Fischer and Stevenson, 1973; Fischer, 1977]. Natural hydrocarbon seeps should be viewed as dynamic systems which are continually evolving. However, the time scale for seep evolution is not well constrained. There may be various processes operating simultaneously at different rates and dependent on a variety of environmental factors.

Fischer [1977] suggested an evolutionary sequence of young, predominantly gaseous seeps venting off, gradually becoming increasingly oily, and eventually being preserved as tar mounds. Vernon and Slater [1963] observed submarine tar mounds SCUBA diving along the northern flank of the Santa Barbara basin and noted some oil and gas emerging from tar mound vents, but more commonly issuing from nearby sand or rock fractures. They suggested viscous residual tar left by escaping oil eventually sealed the seepage fracture conduits, subsequently altering seep distribution.

The effects of subsea weathering would also cause progressive alteration of submarine seep products from oil to tar. The weathering process includes mechanisms summarized by Hunt [1979] such as leaching of water solubles, microbial degradation, polymerization or combining of some molecules into larger structures, and gelation, the formation of a rigid gel structure. Non-marine surface seeps also lose volatile hydrocarbons through evaporation and auto-oxidation from exposure to air and sunlight.

Other factors may control the variation in seepage. The subsurface hydrocarbon accumulations feeding seeps may dry up, or erosion might expose new accumulations previously sealed within the subsurface. Structural changes could open new migration pathways within the seep plumbing system. Seismic activity would exert an important influence in opening new meshes of faults and fractures which would enhance fluid flow. Fischer and Stevenson [1973] comment on the apparent correlation between earthquake activity and seepage at Coal Oil Point. Wilkinson [1972] offers anecdotal evidence of an episodic methane gas seep introduced offshore of Malibu following a major earthquake centered in the San Fernando Valley in 1971. Wilkinson states the

cause was apparently an earth movement which fractured the Monterey Shale bedrock thinly overlain by a layer of unconsolidated sediment.

Other types of episodic seepage events could accompany migratory earthquake swarms [Sibson, 1996] or result from sediment degassing to the water column due to storm surges or mud diapirism [Hovland, 1993]. Such activity would be ephemeral in nature, comprised of sporadic events. On the other hand, changes in seep plumbing resulting from blockage of seepage pathways, seismically induced structural changes, exposure by erosion or burial by deposition would tend to irreversibly alter seep distribution. This illustrates the extremes over which changes in seep distribution can occur, from transitory events to permanent alterations.

Cyclic variations in seepage may also operate between these two extremes. Seasonal changes or tidal cycles have been hypothesized to cause periodic oscillations in seepage rates. Wilkinson [1972] states some observers claim flow volumes of oil from Coal Oil Point seeps increase during the summer months, although he does not quantify this observation. Possible causes for this phenomena would include the decrease in oil viscosity and solubility of methane gas with increasing water temperature. Mikolaj and Ampaya [1973] claimed that increased tidal height decreased seepage of oil at the nearshore Isla Vista seeps just off Coal Oil Point which they attributed to the increase of the hydrostatic head. Hovland *et al*. [1993] cite reduction in hydrostatic pressure associated with ebb tide triggering ebullition of methane from supersaturated pore waters. Such intermittent oscillations based on seasonal or tidal cycles could vary seep emission volumes in addition to episodic seepage events or permanent changes altering seep distribution.

Anthropogenic effects could also affect seep distribution patterns and emission rates over time. Many authors point to the effect of oil production in reducing seepage rates [Fischer and Stevenson, 1973; Landes, 1973; Fischer, 1977; Kvenholden and Harbaugh, 1983]. Numerous examples throughout the world demonstrate a reduction in natural hydrocarbon seepage associated with oil production. The reduction of reservoir pressure associated with production is one possible mechanism for causing seepage to dry up. Fischer and Stevenson [1973] propounded this hypothesis for the Coal Oil Point seeps. On the other hand, production may simply remove leaking hydrocarbons from the subsurface. Landes [1973] offers examples of the Kirkuk field in Iraq and Mene Grande in Venezuela where natural seeps have diminished as production has drawn down hydrocarbons in the reservoirs. Kvenholden and Harbaugh [1983] offer the example of Pitch Lake on Trinidad which once provided a continuous flow of asphalt into the Gulf of Paria until mining lowered the lake below its outlet.

In alluding to the role of man’s activities in reducing hydrocarbon seepage into the marine environment worldwide, Kvenholden and Harbaugh [1983] point to the previous examples which they state “document the assertion that continued production of petroleum should cause seepage rates to decrease in the future”, but they also point out that in some cases “secondary recovery methods using increased formation pressures could possibly cause increased rates of oil seepage”.

Wilkinson [1972] relates the sequence of events leading to one such man made oil seep during the 1969 oil spill in Santa Barbara:

> "On January 29, 1969, a well being drilled from (Union Oil Company's) platform "A" penetrated a high pressure zone below 3,400 feet. Gas from this zone started flowing up the well bore to the surface. The well was closed in and remained temporarily under control, but pressure continued to increase within the well until gas-charged drilling fluid finally broke through the uncased portion of the hole into the shallow oil sand lying just below the sea floor. The gas soon permeated the sand apparently forming fissures through which the now gas-saturated oil literally erupted from the sea floor forcefully expelling oil and gas into the sea."

This example illustrates the potential for anthropogenic effects associated with oil production altering rates and distribution of hydrocarbon seepage. In this case gas formed fissures provided the fracture pathways and the seepage was driven by a high pressure gas zone, which highlight the possibility that similar mechanisms may be responsible for natural seepage. Although the immediate effects of this oil spill were severe, with flow rate estimates from 500 to 5,000 barrels per day (80,000-800,000 liters/day), long term effects of the spill were negligible and recovery of the area complete [Straughan and Abbott, 1971].

For the seeps in the Coal Oil Point area, oil production is most likely responsible for a long term trend of decreasing seep emissions coinciding with a progressive reduction in the area covered by seepage [Fischer and Stevenson, 1973; Fischer, 1977]. One important goal of this work is to attempt to corroborate this hypothesis but in a more rigorous way using quantified estimates of seep emissions and variations.

5.1 NATURAL HYDROCARBON SEEPAGE AT COAL OIL POINT, CALIFORNIA

W. P. Blake of the U. S. Geological Survey, an early explorer of the western United States, commented on natural marine hydrocarbon seepage in the Santa Barbara Channel in 1853, "I am informed ... that the channel between Santa Barbara and the islands is sometimes covered with a film of mineral oil." [Hunt, 1979]. It is quite likely that this reference referred to seepage in the vicinity of Coal Oil Point. Early explorers and Spanish missionaries confirm the long documented historical record of the prolific seepage at this site. For example, Padre Pedro Font wrote in 1776 while near Goleta: "Much tar which the sea throws up is found on the shores ... perhaps there are springs of it which flow out into the sea." [Wilkinson, 1972; Fischer, 1977], and Captain Cook's navigator Vancouver wrote in his journal while anchored off Goleta in 1793: " ... the sea had the appearance of dissolved tar floating on its surface, which covered the ocean in all directions within the limits of our view ..." [Fischer, 1977]. In addition, Native American Chumash in the Santa Barbara area were known to utilize seep tar for caulking canoes and waterproofing baskets at least 7,000 years ago, well before the arrival of westerners [Wilkinson, 1972; Fischer, 1977].

References to the Coal Oil Point seeps are also abundant within the scientific literature [Vernon and Slater, 1963; Allen *et al*., 1970; Wilkinson, 1972; Fischer and Stevenson, 1973; Mikolaj and Ampaya, 1973; Wilson *et al*., 1974; Fischer 1977; Reed and Kaplan, 1977; Kvenholden and Harbaugh, 1983; Hovland *et al*., 1993]. Wilson *et al*. [1974] note in general the paucity of data on offshore seeps throughout the world due to insufficient exploration, but the Coal Oil Point seeps are an exception, and probably the most studied in the literature.

The Coal Oil Point seeps are located along the northern flank of the Santa Barbara basin (Figure 1). This is a typical environment with high seepage potential [Link 1952; Wilson *et al*., 1974], the margin of a basin with known petroleum accumulations and strike slip faulting and tight compressive folding associated with a high incidence of earthquakes. The bedrock of the northern shelf is predominantly Miocene age siliceous and diatomaceous shales and silts of the Monterey and Sisquoc Formations onlapped at the seaward edge by the Pliocene age Repetto and Pico Formations [Vernon and Slater, 1963; Fischer and Stevenson, 1973; Fischer, 1977]. A variable thickness veneer of unconsolidated late Quaternary silts, sands, and conglomerates rests unconformably atop the bedrock. The fractured Monterey Formation is both source and reservoir rock for hydrocarbons [Isaacs and Peterson, 1987] and is the source of the seep oil and gas at Coal Oil Point [Reed and Kaplan, 1977; Hartman and Hammond, 1980].

Figure 1: Location map of the study area.

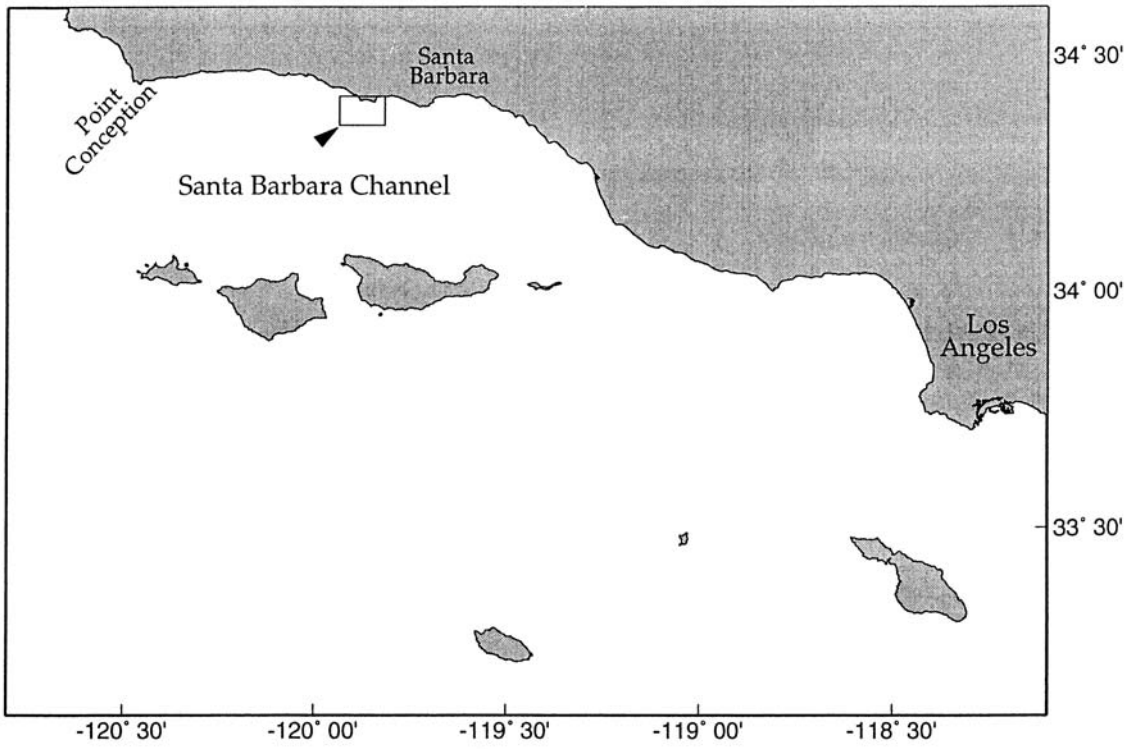

Seep trends (Figure 2) align with dominant east-west structural features which parallel the tectonic grain of the Western Transverse Ranges. Faulted east-west trending anticlines correlate with tar seeps from fractures in Miocene siliceous shales near Point Conception [Vernon and Slater, 1963], and elongated seepage structures in the Coal Oil Point area also parallel anticline

crests (Figure 3) [Fischer and Stevenson, 1973; Fischer, 1977]. Dense networks of crestal fractures within the anticline axes are indicated by the absence of seismic reflections [Fischer and Stevenson, 1973], and inferred to be seep conduits for vertical fluid migration. Faulting is assumed to be an important mechanism for introducing the secondary porosity of these fracture networks, and high angle cross faults may serve as additional seep pathways [Fischer, 1977]. This could lead to “bright spots” of intense seepage where faults intersect anticline axes, and fault splays may cause irregular deviations from the linear seepage trends [Fischer, 1977].

Figure 2: Compilation of seep distribution from 1946-1976, after [Fischer, 1977]

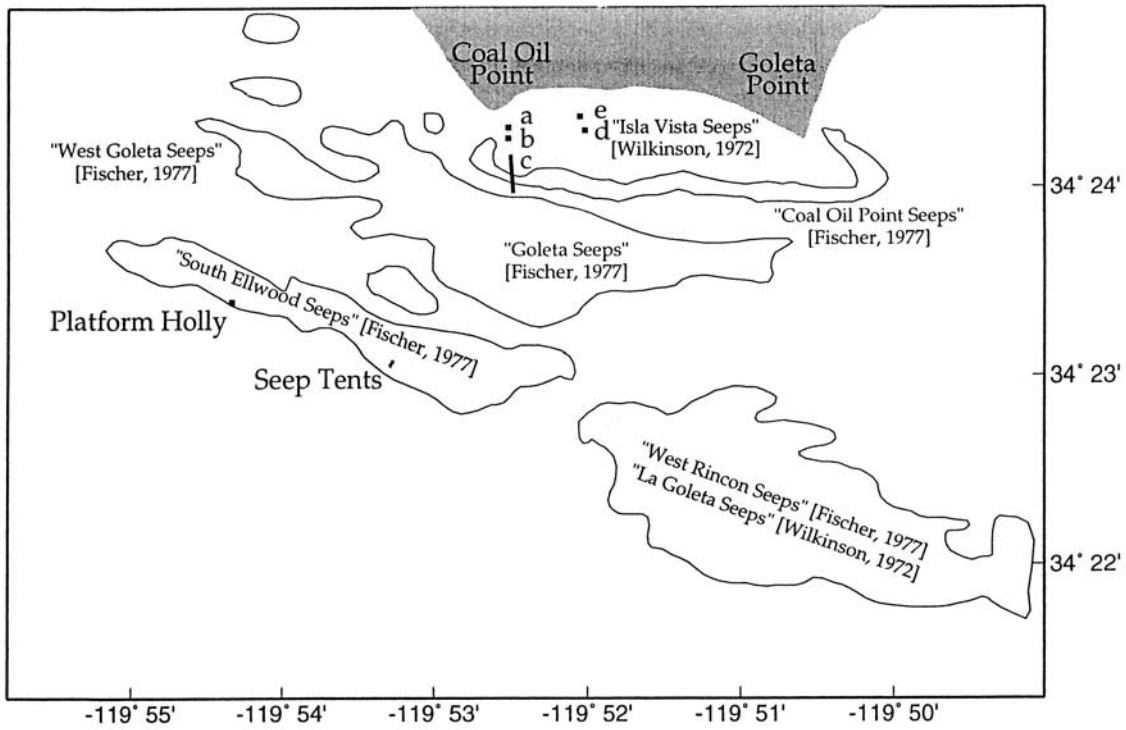

Figure 3: Submarine geologic structure offshore Coal Oil Point.

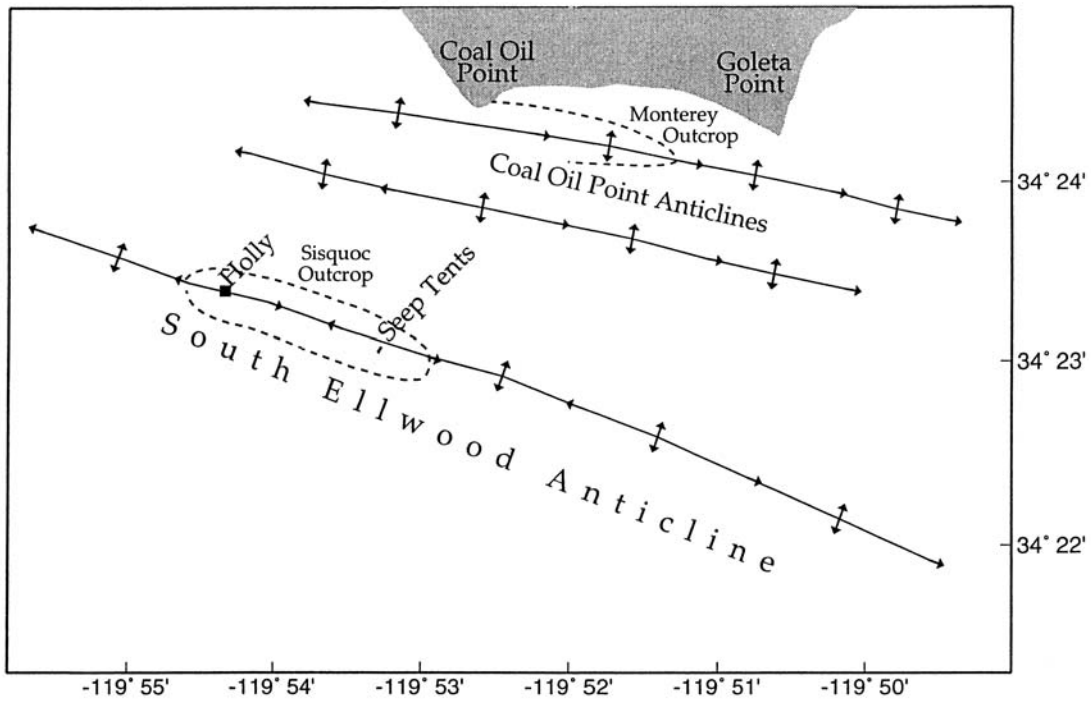

Thickness of the overburden of unconsolidated Quaternary sediment has also been suggested to control the distribution of seepage [Fischer and Stevenson, 1973; Fischer, 1977]. However, since sediment cover tends to truncate over structurally controlled topographic highs such as anticlinal axes [Fischer, 1977], it is possible that this trend indicates the structural influence governing seepage rather than demonstrating a causal effect of its own.

Figure 2 shows a comprehensive map of seep distributions in the Coal Oil Point area compiled using oil company data from 1946-1947 and 1953-1956, and sonar data from 1972-1973 as presented by Fischer [1977]. It should be noted that by combining the data sets, the map fails to illustrate the erratic variations in seep distribution claimed by Fischer [1977] which he attributed to the intermittent nature of seepage, but which could also arise from different coverage of the surveys, or navigational errors. However, the map does demonstrate the linear east-west trends of seepage which Fischer [1977] described.

There is no consistent naming convention in the literature regarding the seep areas mapped in Figure 2. The entire map view area has been collectively termed the “Coal Oil Point Seeps” [Wilson *et al*., 1974; Kvenholden and Harbaugh, 1983; Hovland *et al*., 1993], but Fischer [1977] referred to the “Coal Oil Point Seeps” as the nearshore trend while Wilkinson [1972] designated the “Coal Oil Point Seeps” in the area of a, b, and c in Figure 2. Labels a, b, c, d and e in Figure 2 represent the sites of measurements by Allen *et al*. [1970]. The study of Mikolaj and Ampaya [1973] was confined to the area of d and e, termed the “Isla Vista Seeps” by Wilkinson [1972].

Other names include “La Goleta Seeps” [Wilkinson, 1972] or “West Rincon Seeps” [Fischer, 1977] for the large seep to the southeast of the map, “Goleta” and “West Goleta” [Fischer, 1977]

for the irregular seep in the middle of the map, and “South Ellwood Seeps” [Fischer, 1977] in the area around Platform Holly and the Seep Tents. Holly is an offshore oil platform producing from the Monterey reservoir through Sisquoc cap rock. The Seep Tents are a pair of large steel pyramids approximately 100 m^2 at the base installed on the seafloor by ARCO in 1982 to cap a particularly active area of seepage [Rintoul, 1982; Guthrie and Rowley, 1983].

Figure 3 shows the structural features which correlate with the seep trends presented in Figure 2. Immediately offshore the Coal Oil Point Anticline defines the seepage trend studied by Allen *et al*. [1970] and Mikolaj and Ampaya [1973], who observed oil globules exuding from discrete openings through the unconsolidated sediment overlain on a bottom topography of fractured shale. The Monterey formation outcrops at the seafloor here in the axis of the Coal Oil Point Anticline [Fischer, 1977]. These nearshore seeps are predominantly oil and tar seeps similar to those in the Point Conception area [Vernon and Slater, 1963], whereas the outer seep trends further offshore tend to be dominated by roughly equal parts of oil and gas [Fischer, 1977]. This increase in the ratio of gas to oil moving offshore may reflect stages of seep evolution [Fischer, 1977], with gas venting off from the relatively younger seeps which become increasingly dominated by oil as they mature. Alternatively, this may reflect that while inshore oil seepage occurs directly from the Monterey Formation reservoir, further offshore gas buoyancy is required to provide a driving mechanism for transport through the Sisquoc cap rock.

Outside of the inner Coal Oil Point Anticline a second anticline unknown to Fischer [1977] coincides with the central trend of seepage in Figure 2. These paired anticlines interpreted as the Coal Oil Point fold complex [Bartsch *et al*., 1996] culminate just south of the point, where persistent seepage has occurred in the past [Fischer, 1977]. The central seepage trend corresponds to where the second anticline axis and synclinal limbs intersect the seafloor, and may be most intense where axial surfaces are cut by cross faults [Bartsch *et al*, 1996], as suggested by Fischer [1977]. The linear feature c in Figure 2 described by Allen *et al*. [1970] lies along the projection of an onshore-offshore fault striking N15°W and dipping 45° east [Fischer and Stevenson, 1973; Fischer, 1977].

The outermost seep trends align with the axis of the South Ellwood Anticline (Figure 3). This is a multiple plunging anticline with a series of structural culminations which control the distribution of seepage. Bore hole data suggest that maximum seep intensity following the trend of the axial surface correlates to locations where the Sisquoc/Monterey formation contact is more shallow [Bartsch *et al*., 1996]. One culmination lies beneath Platform Holly, a second beneath the Seep Tents, and a third in the center of the La Goleta seep field, each of which was a location of intense historical seep activity [Fischer, 1977]. Due to this structural relief, Sisquoc outcrops on the seafloor around Platform Holly and the Seep Tents along the South Ellwood Anticline axis. The structural saddle along this axis may also be responsible for the separation between the two outermost seepage trends in Figure 2 [Fischer, 1977].

5.2 PREVIOUS ESTIMATES OF SEEPAGE FLOW RATES AT COAL OIL POINT

Previous quantitative estimates of seepage in the Coal Oil Point Area have been made [Allen *et al*., 1970; Mikolaj and Ampaya, 1973; Fischer, 1977], but the inherent inaccuracies in these estimates are acknowledge by the authors given the difficulties involved in such measurements and the possibility that seep rates could fluctuate. Allen *et al*. [1970] estimated oil seepage in the nearshore area (a, b, c, d and e in Figure 2) leaked 50-70 barrels/day (8000-11,000 liters/day) with a possible range from 10-100 barrels/day (1600-16,000 liters/day). Mikolaj and Ampaya [1973] estimated oil flow of 12.5 barrels/day (2000 liters/day) confined in the area of d and e. These studies were concerned only with rates of oil leakage and not gas. Fischer [1977] determined flow rates of liquid oil for the entire offshore area of seepage would be 55 to 800 barrels/day (8800-12,800 liters/day) based on the local rates of Allen *et al*. [1970], but allowing for the higher gas fraction in the outer seep trends would revise this estimate to 25-400 barrels/day (4000-64,000 liters/day) [Fischer, 1977]. Estimates for the emissions of gaseous hydrocarbons from seepage are also available. Hovland *et al*. [1993] estimated a methane flux of 400 g m^{-2} yr^{-1} from the Coal Oil Point area based on the volume of gas collection at the Seep Tents (a point source) distributed over the 18 km^2 area surveyed by Fischer [1977], and Saxena and Oliver [1984] estimated 18 to 152 tons of ROG's per day are produced by all the Santa Barbara Channel seeps.

6.1 OCEANOGRAPHIC SURVEYS

To map the distribution of gas seeps offshore of Coal Oil Point for this study, a series of marine surveys were undertaken in 1994, 1995, and 1996. Locations of gas seeps associated with the offshore seepage trends were pinpointed with acoustic reflection systems which sense the presence of gas bubbles in the water from the density contrast between seawater and these bubbles [Sweet, 1973; Tinkle, 1973]. Accurate navigation was insured with differential GPS. The inshore oil seeps were not mapped for several reasons: the shallow inshore water and kelp presented logistical problems for the survey boats, oil seeps lack the distinctive acoustic signature of gas seeps since density contrast between oil and water is low, and the inshore oil seeps have already been extensively studied in the past.

Two different frequency acoustic systems, one 50 kHz and the other *3.5* kHz, were utilized for the surveys. Since frequency response of the sonar is dependent on bubble size distribution, data for the different surveys is not completely comparable. The 3.5 kHz sonar would have a stronger return but be more non-linear based on the location of the resonance peak with respect to the observed distribution of bubble sizes (see Section 8.1).

The 50 kHz acoustic source was a hull-mounted Raytheon wide-beam transducer (model MCPT 25-05) operated from the *Genoa* out of Santa Barbara Harbor. The analog signal was recorded with a Raytheon JRC JFF-770 paper chart recorder. The 50 kHz surveys were conducted November 20, 1994; December 27, 1994; August 15, 1995; and November 15, 1995. Cruising speed for surveys aboard the *Genoa* varied between 5.6 and 8.4 knots, with an average cruising speed of 7.0 knots. The resulting vertical exaggeration of the paper records was approximately 40:1 given the chart recorder speed.

The 3.5 kHz acoustic source was a towfish-mounted transducer deployed from the *Seawatch*, a vessel in the fleet of the Southern California Marine Institute operating out of San Pedro, California. The transducer was towed at a depth of 10 m at a cruising speed of approximately 5 knots. Analog records were recorded simultaneously using both a Gifft-type wet paper recorder and an EPC dry (thermal) paper recorder. In addition, digital data was collected using a SUN IPX workstation equipped with an A/D Board and digitizing software developed at the University of Hawaii. The A/D was triggered by the same recorder that triggered the transducer. The digitization rate was 10 kHz (0.1 msec sample period). The transceivers were operated without time varied gain (TVG), and a Krone-Hite filter bandpassed the signal from 3 to 4.8 kHz to eliminate excess noise. The 3.5 kHz surveys were conducted July 26-27, 1995; September 28-30, 1995; and August 15-17, 1996. In addition to this newly acquired data, historical 3.5 kHz analog paper records from surveys made by Peter Fischer in 1972 and 1973 were obtained for the purpose of comparing the change in seep distribution over a 20 year time period.

6.2 METHOD OF MAPPING SEEP DISTRIBUTION

The acoustic data acquired during the marine surveys offshore Coal Oil Point provide a cross section of the water column and sub-bottom along the navigational track of each survey. The delay time of each successive acoustic pulse is related to the depth within the cross section by the sound speed, which is approximately 1500 m/s for the seawater and water saturated seafloor sediments. Figure 4b illustrates a sample cross section of the water column and sub-bottom for a line running roughly west-east from the location of the Seep Tents to the La Goleta Seep field along the axis of the South Ellwood Anticline (location of the cross section line in map view is shown in Figure 5). This particular cross section is digitally recorded 3.5 kHz data from the August 1996 cruise.

Figure 4: (a) Normalized intensity profile calculated by 6.2.1 for the water column cross section shown in (b). The dark columnar bands are gas seeps along the cross section line in Figure 5.

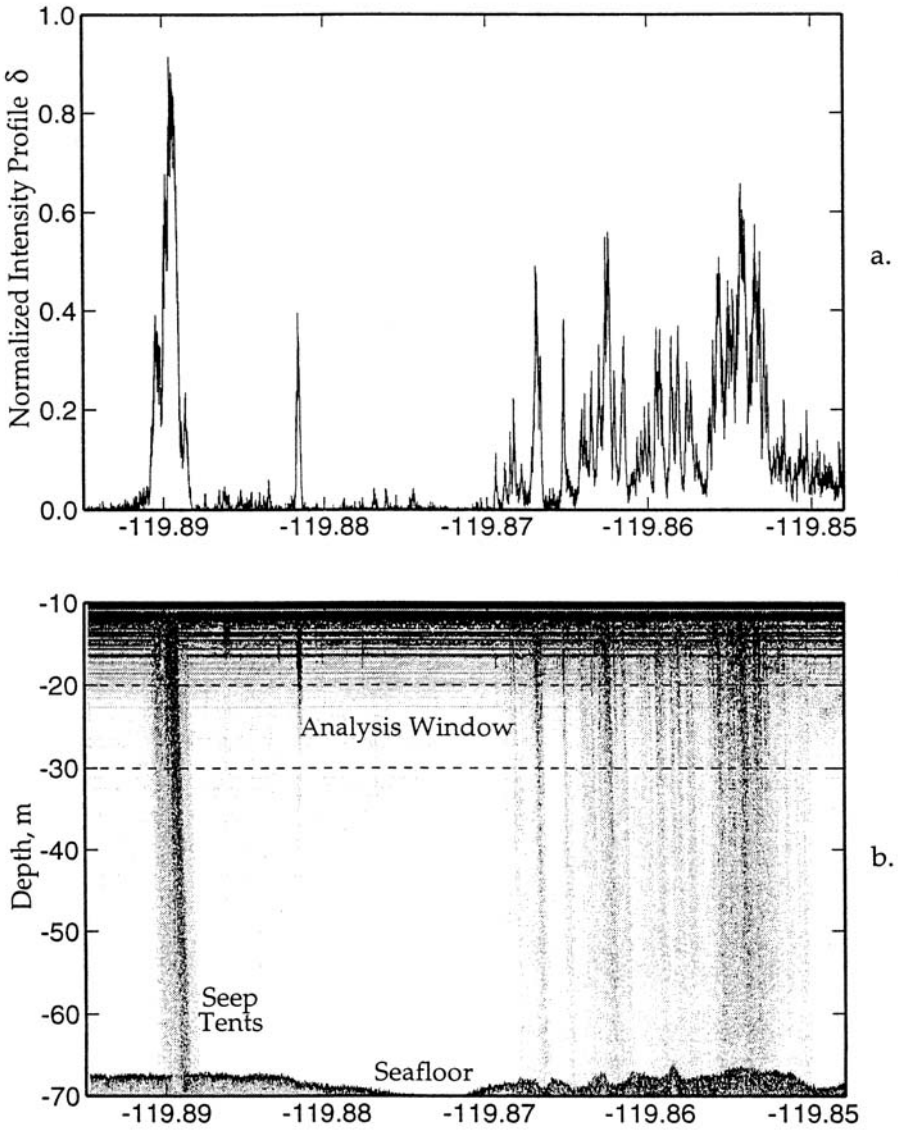

Figure 5: Distribution of seepage mapped from relative intensity values contoured above 0.05 for digitally recorded 3.5 kHz data from August 1996.

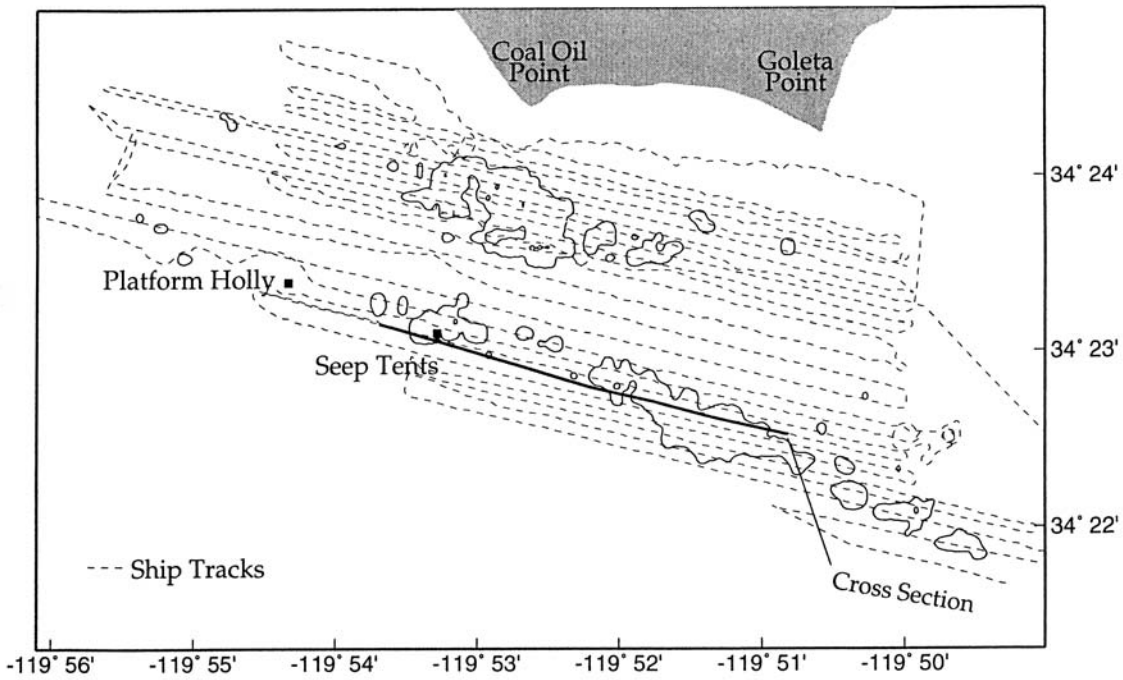

The dark columnar bands within the water column are representative of gas seeps. In the case of analog paper records, the paper scrolls were scanned on an HP Deskjet scanner at 200 dpi resolution to acquire 8 bit digital images which could be processed in a similar manner to the image displayed in Figure 4b. The resulting scanned images have a grayscale with 256 levels of pixel brightness. Since seeps are represented by dark areas in the images, the grayscale was inverted to darkness by subtracting the brightness value from 255. The scanned analog records have less dynamic range and saturate at a lower level than the digitally recorded data, but offer greater coverage and allow comparison with historical datasets.

To convert the cross section data into a map view plot of seep intensity distribution, a line profile of relative seep intensity was constructed as shown in Figure 4a. The line profile is obtained by scaling the intensity within a 20-30 m depth window of the cross section relative to mean background intensity values and normalizing by the average intensity of the outgoing acoustic pulse which is the dark band across the top of the record. This can be represented in equation form as:

$$\delta = \frac{\alpha - \beta}{\gamma - \beta} \qquad (6.2.1)$$

Here δ is the normalized darkness profile as shown in Figure 4a, α is the intensity within the water column window, β is the mean intensity within the water column window in the absence of seepage, and γ is the mean intensity of the outgoing acoustic pulse.

For the scanned analog images, mean values of darkness were taken as the proxy for intensity. For the digital 3.5 kHz data such as that displayed in Figure 4, the standard deviation of the signal over a given time window was taken as the proxy for intensity. Standard deviation is the root mean square deviation and represents relative energy of the signal since it is equal to the square root of the sum of energy over all frequencies from Parseval's theorem. The range of data for calculating intensity of the outgoing pulse was considered to be the first 50 points of each shot trace, corresponding to the 5 msec pulsewidth of the sonar based on the 10 kHz digitization rate. The range from 125 to 275 points within each shot trace approximately corresponded to the depth window of 20-30 meters in the water column based on two way travel time for a seawater velocity of 1500 m/s and a towfish depth of 10 m.

The relative seep intensity δ profile data, as shown in Figure 4a, were subsequently gridded at 100 by 100 meters. Separate gridded data sets were calculated for the various surveys, both analog and digital, in order to present a series of seep distribution maps over time. The gridded data was contoured using a tension spline surface algorithm [Smith and Wessel, 1990] and displayed as a relative intensity plot of seep distribution. An estimated threshold level for the first contour above the level of noise was selected as 0.05 for the digital data and 0.1 for the scanned analog data.

7.0 SEEPAGE DISTRIBUTION MAPS

The seep distribution displayed in Figure 5 for the August 1996 3.5 kHz digital data is similar to the distribution reported by Fischer [1977] (Figure 2) with respect to the various structural trends (Figure 3), but the coverage is not as extensive as his. Note that the Coal Oil Point seep trend mapped by Fischer [1977] (Figure 2) represents oil seepage and should not be directly compared to Figure 5 which plots the distribution of gaseous seepage. The seepage due south of Coal Oil Point in Figure 5 between 34°23' and 34°24' North and -ll9°52 to -1l9°54' West is not as extensive as the Goleta seepage trend reported by Fischer [1977] (Figure 2). However, Fischer [1977] claims seepage within this trend was intermittent on the 10 to 20 year time scale between the surveys on which he based his map, acquired from 1946 to 1977, with the most consistent seepage occurring in the area we show due south of Coal Oil Point (Figure 5).

The outer seepage trends are also less extensive and noncontiguous in Figure 5 as compared with Figure 2. In particular, part of the South Ellwood seep trend is absent in the area to the west around Platform Holly, and the West Rincon or La Goleta seep trend identified in Figure 2 is more tightly confined along the anticline axis. Fischer [1977] proposed a progressive shrinking in the extent of seepage based on his own comparison of data from 1946-47, 1953-56, and 1972-73 (1976); the August 1996 3.5 kHz digital data (Figure 5*)* appears to corroborate his hypothesis. However, Fischer [1977] does not rigorously define his method for judging what constitutes seepage or describe how he arrived at the seep distribution mapped in Figure 2. In addition, navigational techniques available for the historical surveys of the seeps were less accurate and precise than modern differential GPS. Therefore, the accuracy of the seep distribution in Figure 2 is unknown.

To allow a more one-to-one comparison of seep distribution as mapped by Fischer with the distributions determined from our own surveys, the 3.5 kHz analog scrolls acquired by Fischer in

1972-73 were borrowed and scanned to obtain these analog records in a digital file format. To make the comparison more direct, our own Figure 6 shows the comparison of seep distribution plotted from analog 3.5 kHz data collected by Fischer in 1973 (Figure 6a) and our survey in July 1995 (Figure 6b) along the axis of the South Ellwood Anticline. The box on the map outlines the 13 km^2 region where the navigational coverage is similar, and track lines from which data from the two surveys are plotted are also shown. Figure 7 shows the same comparison, but within the 13 km^2 boxed region of Figure 6. From Figure 7 it is apparent that the distribution of gaseous seepage decreased within a few kilometers of Holly over the 22 year time period spanned from 1973 to 1995.

Figure 6: Comparison of (a) 1973 3.5 kHz survey data from Fischer and (b) July 1995 3.5 kHz survey contoured at 0.1 relative intensity level. Boxed region represents area with similar navigational coverage.

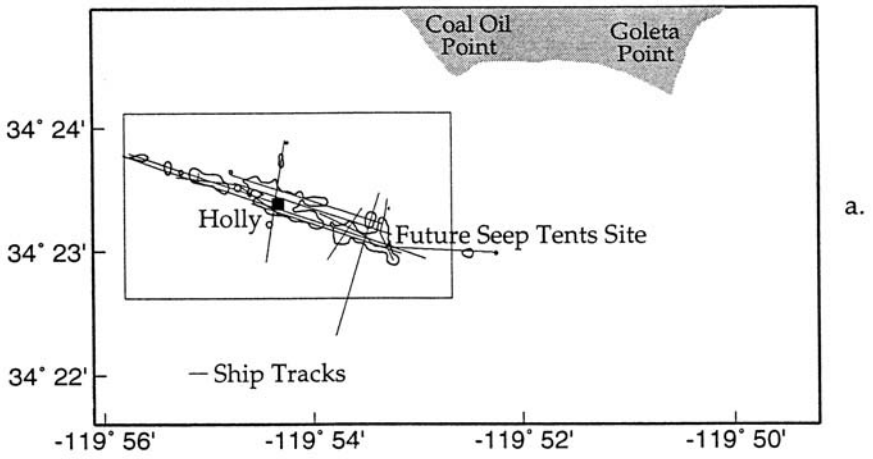

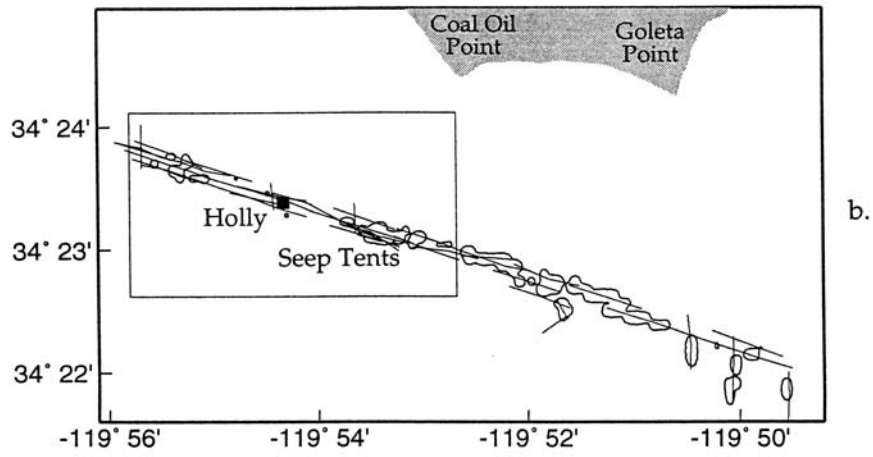

Figure 7: Comparison of (a) 1973 3.5 kHz data from Fischer and (b) July 1995 3.5 kHz data contoured at the 0.1 relative intensity level within the boxed region from Figure 6.

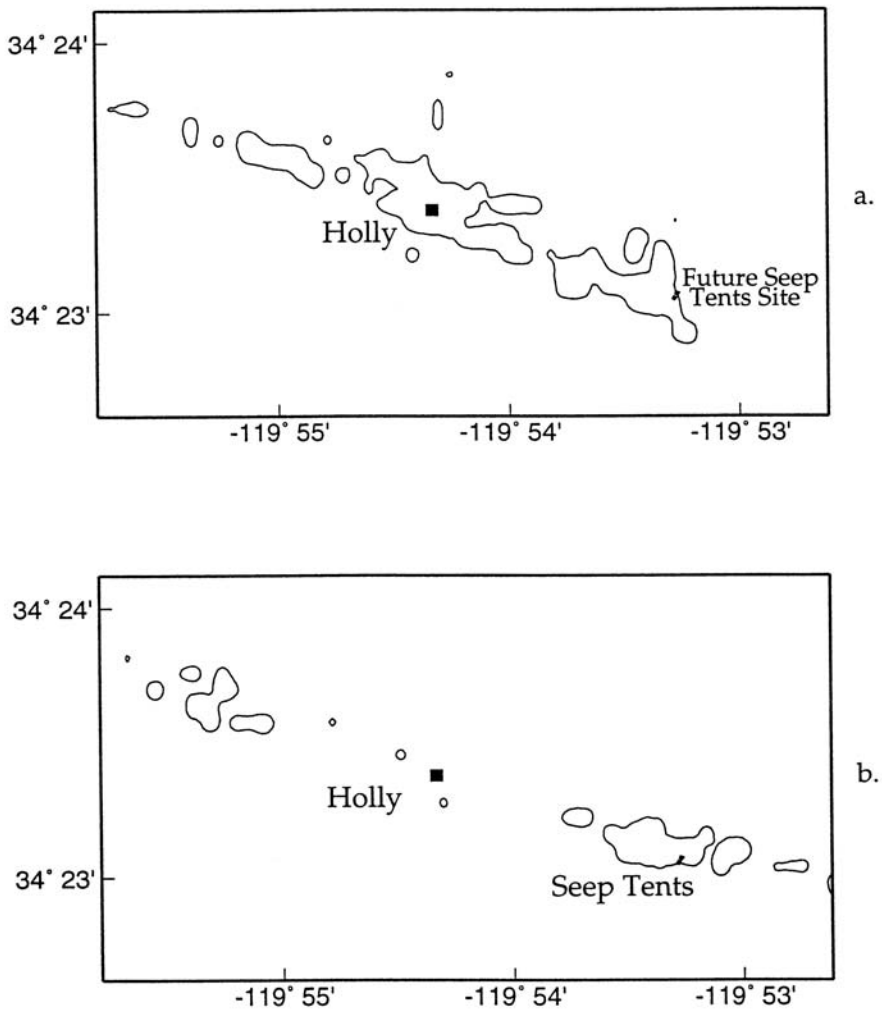

Fischer [1977] stated that a progressive decrease in the extent of seepage occurred offshore Coal Oil Point due to oil production from Holly. This seems to imply shrinking inward of the seep trends toward the platform. However, what is actually observed in Figure 7 is the disappearance of seepage outward from the platform while peripheral seepage is left intact. The observed decrease in seepage outward away from Holly contradicts slightly Fischer's [1977] original statement. However, this could be explained as the result of oil production from platform Holly gradually being pushed further and further afield. On the other hand, if one is to believe the accuracy of the seep distribution mapped by Fischer [1977] (Figure 2) going back to the 1950's, then Fischer's statement is true for other seep trends in the Coal Oil Point area but not for those in the immediate vicinity of Holly.

Since the comparison with Fischer's data was only valid within a limited portion of the survey area, we also conducted comparisons of our own data sets for the series of surveys that we had

acquired. Figure 8 shows the distribution of seepage compiled from 3.5 kHz analog and digital data obtained in the summer of 1995 during July and September. The combined coverage of these surveys, as shown by the track lines, contains a few gaps compared to the coverage in August 1996. This may explain some of the differences between the seep distributions displayed in Figure 5 and Figure 8. An example is the gap in the 1995 coverage roughly due south of Coal Oil Point (Figure 8). Although GPS navigation insures that seeps are accurately located, gaps and holes in the plots of seep distribution should be considered suspect where coverage is absent.

Figure 8: Distribution of seepage mapped from relative intensity values contoured above 0.05 for digital 3.5 kHz data from Sept 1995, and analog and digital 3.5 kHz data from July 1995.

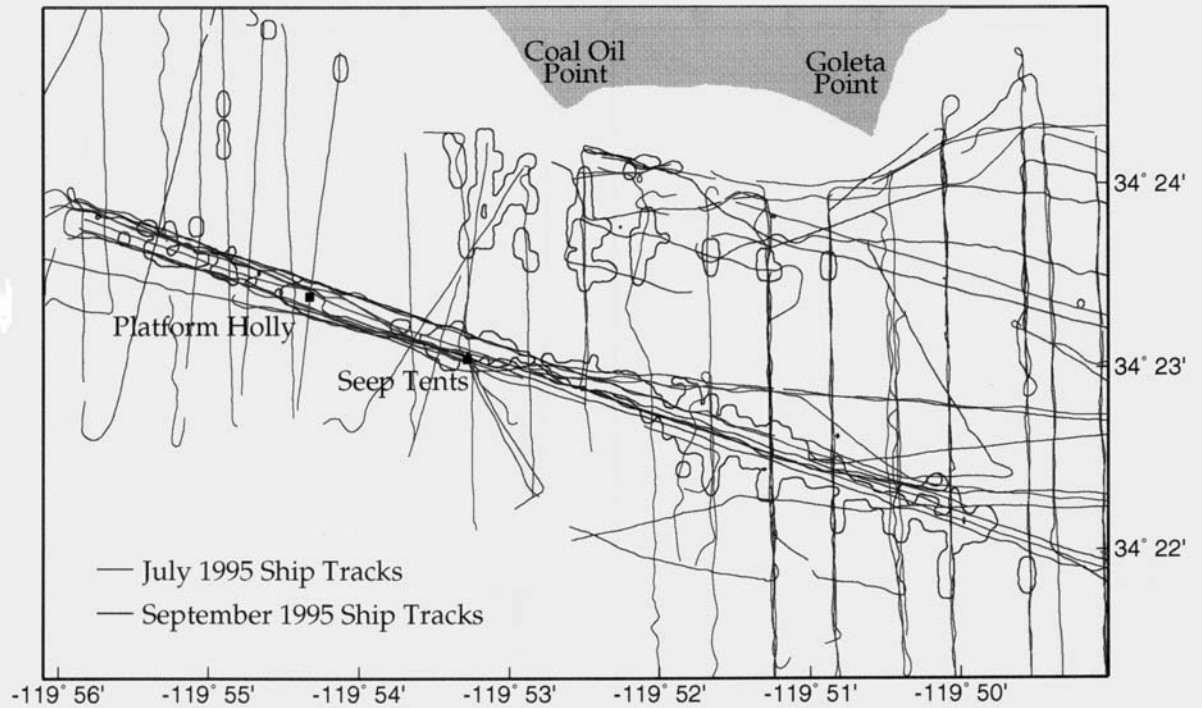

Furthermore, since our method for locating gas seeps maps bubbles at 20-30 m depth within the water column rather than at the seafloor source, the shearing effect of water currents visible in cross section is expected to shift the displayed distribution of seepage west-southwest of the seep sources given the predominantly westward local current flow which shifts slightly south with ebb tide [Fischer, 1977; Kolpack, 1977]. Given bubble rise velocities (see Appendix 1) and maximum current velocities [Fischer, 1977] are on a similar order of about 20 cm/sec, seep bubbles would be expected to shift a horizontal distance on the order of the water depth by the time they reach the sea surface, implying a maximum shift in position of approximately 30 m by the time the bubbles reach the 20-30 m depth window from a typical 60 m depth.

Figure 5 and Figure 8 are similar but with some differences. Both distributions show the dominant La Goleta, or West Rincon, seepage trend along the South Ellwood Anticline axis as well as an amorphous region of seepage to the south of Coal Oil Point. Meanwhile seepage

around Holly is absent, suggestive of the long term change in seep distribution demonstrated in Figure 6 and Figure 7. Neglecting the seeps south of Coal Oil Point where different coverage precludes a comparison, the seep distribution along the South Ellwood Anticline Axis appears to remain relatively stable over a one year time scale but with some fluctuations. For example, the tongue of seepage east of the Seep Tents in Figure 8 is absent in Figure 5, as is the seepage west of Holly, although this may have been skirted by the August 1996 navigation.

Short term changes in seep distribution may occur in addition to long term variation, but an appropriate cause for explaining these changes is currently unavailable. Wilkinson [1972] proposed seasonal variations might affect seep distribution, but both Figure 5 and Figure 8 present seepage during the summer months, and although episodic seepage events could also provide an explanation there is no evidence of activity, such as an earthquake, which might trigger such an event during this time period.

Another short term process previously proposed to affect seepage is tidal forcing. Mikolaj and Ampaya [1973] claimed a correlation between the tidal height, or hydrostatic head, and flow rates of oil at the inshore Isla Vista Seeps (d and e in Figure 2). This would tend to cause cyclic variation in seep emission rates. To examine if emission from gas seeps varied with tidal height, similar profile lines collected at high and low tide were compared. Such a comparison of profiles for two 50 kHz survey lines collected through the intense La Goleta seep field is shown in Figure 9a with the corresponding navigation displayed in Figure 9b. The high tide data was collected at approximately 10:00 am local time on November 20, 1994 while the high tide at Santa Barbara Harbor on this day peaked at 5.8 feet (1.8 m) at 9:18 am. The low tide data was collected approximately at noon on December 27, 1994; low tide on this day at Santa Barbara Harbor peaked at 0.6 feet (0.2m) at 12:05 pm. The difference in tidal height for the two records was therefore approximately 5 feet (1.5m).

Figure 9: (a) Comparison of 50 kHz relative intensity profiles along a similar track at high tide (November 1994) and low tide (December 1994). Divergence of track lines to East shown in (b) may explain some difference.

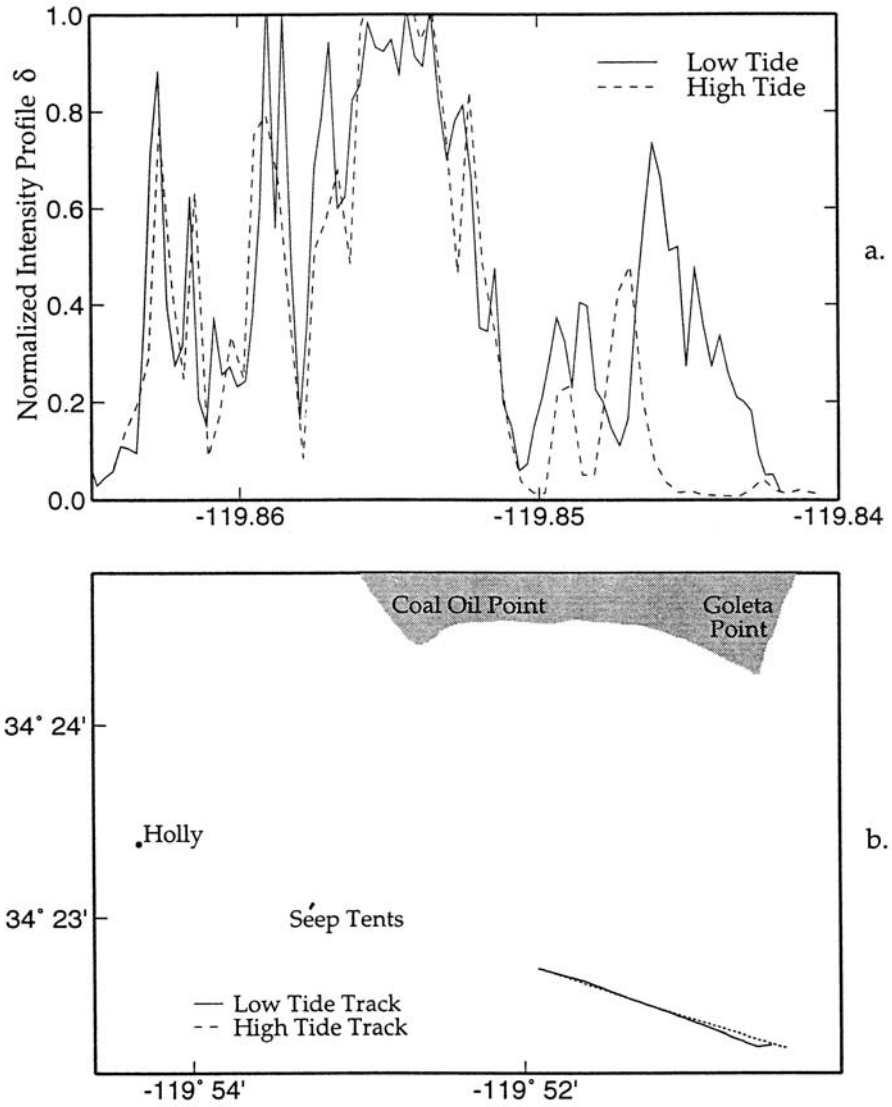

The two profiles in Figure 9a appear similar in detail in the left half of the plot, albeit with some slight shift. The right half of the plot shows some variation with a larger emission at low tide. However, this may be due to slight divergence of the two track lines to the west as shown in Figure 9b. Also, since the tracks were taken approximately one month apart, variations other than those caused by tide may be present. However, other compared profiles, including those compared for different tidal heights on the same day, appeared quite similar to the profiles in Figure 9a. If the profiles of relative sonar intensity obtained using equation (6.2.1) are an accurate representation of relative volumes of seep emission, it would appear that volume emission rates of gaseous seeps are relatively insensitive to tidal cycles. In addition, emission remained relatively constant over the one month time period between November 20, 1994 and December 27, 1994.

It may be that short term variations in seep distribution are a second order effect in comparison to the type of long term variation illustrated in Figure 6 and Figure 7. This assumption was made when compiling July and September 1995 3.5 kHz data into a single plot of seep distribution (Figure 8). Similarly, all the 50 kHz data collected over a one year period during surveys in November 1994, December 1994, August 1995, and November 1995 were incorporated into a single dataset to represent seep distribution averaged over this one year period (Figure 10). In part, combining the different surveys into common datasets was motivated by lack of navigational coverage. Combining different surveys provides more complete coverage to allow better spatial comparisons of changes in seep distribution for the whole Coal Oil Point offshore area. However, at the same time combining the data tends to obscure time variations in seep distribution which may vary for different surveys.

Figure 10: Distribution of seepage mapped from relative intensity values contoured above 0.1 for 50 kHz analog data from November 1994, December 1994, August 1995, and November 1995.

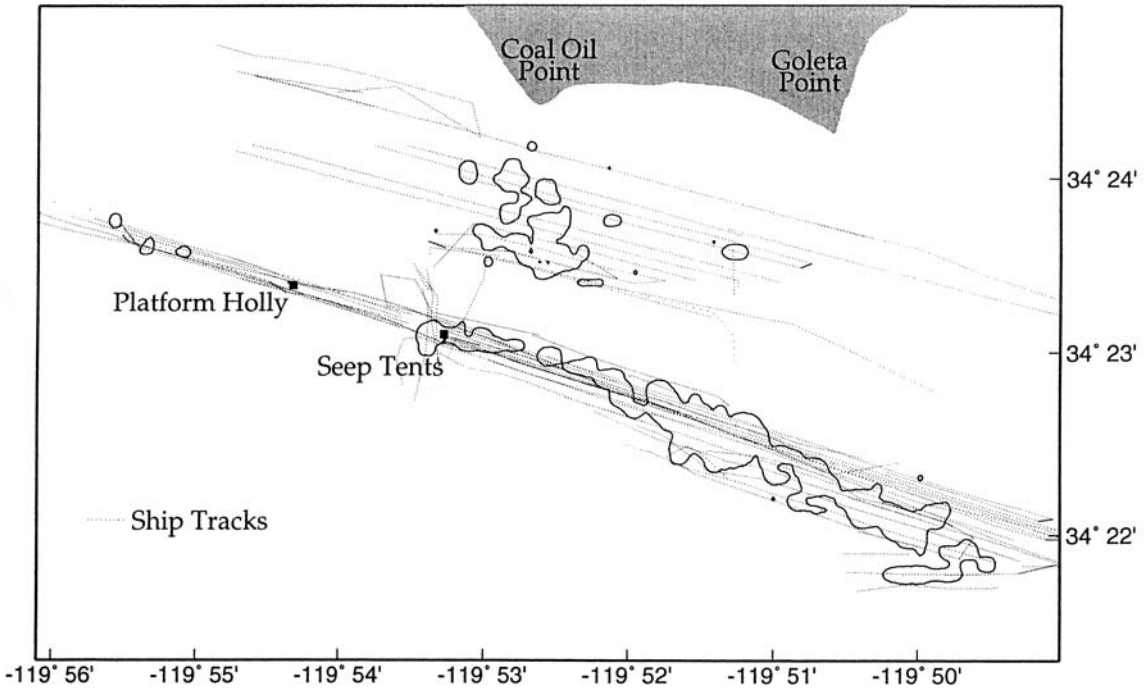

The distributions of seepage based on the August 1996 digital 3.5 kHz data, July and September 1995 analog and digital 3.5 kHz data, and November 1994 through 1995 50 kHz data are plotted together in Figure 11. It is questionable whether comparing data at different frequencies is entirely appropriate since frequency response varies for different bubble distributions as discussed later in Section 8. However, the three surveys do present similar distributions of seepage. The La Goleta or West Rincon seep trend running roughly east from the Seep Tents along the axis of the South Ellwood Anticline is remarkably consistent. The Goleta Seep trend south of Coal Oil Point is more variable, in part due to difference in coverage, but is nevertheless a persistent site of seep activity. Variable seep activity is evident west and north of Holly in the areas previously designated as South Ellwood and West Goleta Seeps [Fischer, 1977] (see Figure 2). The immediate vicinity of Platform Holly is consistently barren of seepage in contrast to 1973 (Figure 6a and Figure 7a).

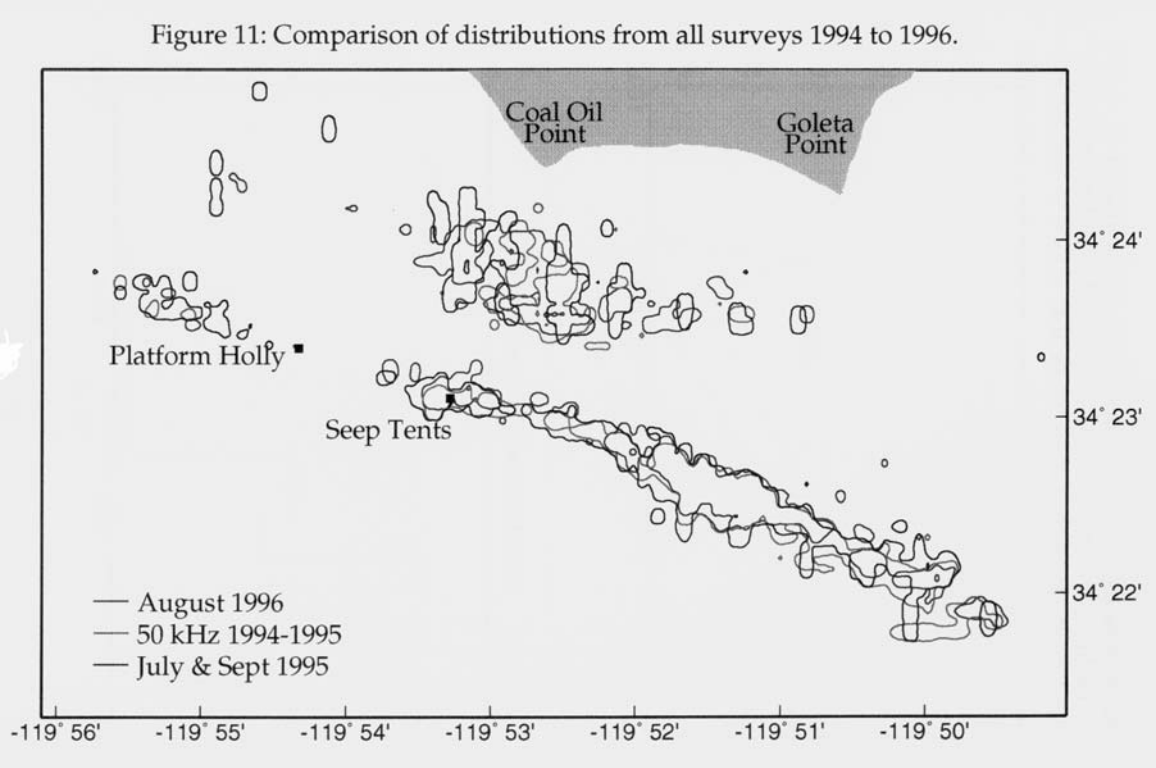

Figure 11: Comparison of distributions from all surveys 1994 to 1996.

The map in Figure 11 seems to suggest that although seepage may be somewhat variable, dominant trends of seepage are remarkably persistent and fairly stable over the short time scale between these surveys. This is in contrast to the long term change demonstrated in Figure 6 and Figure 7. These dominant seepage trends correlate with the told axes shown in Figure 2 and discussed previously in Section 5.1. Previous seepage in the proximity of Platform Holly has apparently disappeared since 1973 which may provide evidence of oil production reducing natural seepage [Fischer and Stevenson, 1973; Fischer, 1977].

8.1 QUANTIFYING SEEP EMISSION RATES - THEORETICAL CONSIDERATIONS

For our study, submarine gas seeps were located by acoustic sensing of the prolific gaseous component of seepage which is so prevalent in the outer seep trends. We also desired to obtain quantified estimates of emission volumes of this gaseous seepage based on our data. Previous estimates of liquid petroleum seepage in the Coal Oil Point area were determined based on the sizes of surface slicks of an assumed thickness and direct collection of oil extruded at the seafloor [Allen *et al.*, 1970; Mikolaj and Ampaya, 1973]. Remote sensing techniques have also been employed to detect surface slicks [Kraus *et al.*, 1977; Estes *et al.*, 1985] and estimate the corresponding oil emission [Clester *et al.*, 1996].

Quantifying the gaseous portion of seepage from our backscattered acoustic data is more problematic and requires calibrating relative sonar return in terms of the rate of gas emission.

Acoustic backscatter from bubble clouds is dependent on both the number and sizes of entrained bubbles, and acoustic frequency [Medwin, 1977a, b; Clay and Medwin, 1977; Urick, 1983]. The frequency dependence of acoustic parameters on bubble radii allows bubble size distributions to be inferred from acoustic backscatter at different frequencies [Vagle and Farmer, 1992]. Backscatter data have advantages over in situ measurements because they can be collected efficiently over relatively large water volumes [Akulichev *et al*., 1986; Vagle and Farmer, 1992]. However, estimating bubble distributions from backscatter data requires a complicated data inversion and involves numerous experimental uncertainties.

For simplicity we consider the active sonar equation in the form used by Vagle and Farmer [1992], equation (2):

$$RL - SL = TS - 2TL \qquad (8.1.1)$$

This equation states that for active sonar, the received level (RL) relative to the source level (SL) is dependent on the target strength (TS) of the reflector and the two way transmission loss (2TL). Transmission loss arising from the presence of bubbles is neglected in equation (8.1.1). Target strength is expressed [Vagle and Farmer, 1992]:

$$TS = \log_{10}\left[\frac{M_\upsilon}{4\pi}\cdot U\right] \qquad (8.1.2)$$

where M_υ is the scattering cross section per unit volume and U is the insonified volume, which depends on characteristics of the sonar such as pulse length, beam pattern (solid angle), and range to the target. If sonar parameters are constant, target strength depends only on scattering cross section per unit volume M_υ, which is defined [Vagle and Farmer, 1992]:

$$M_\upsilon = \int_0^\infty \sigma_s n(a)\cdot da \qquad (8.1.3)$$

σ_s is the acoustic scattering cross section of an individual bubble and $n(a).da$ is the number of bubbles per unit volume with radii between a and $a+da$.

The bubble scattering cross section σ_s has a pronounced peak which is much higher than the geometrical cross section (πa^2 for spherical bubbles) at the radius which corresponds to the resonance frequency with respect to the insonifying acoustic source. Scattering cross section σ_s is given by [Medwin, 1977a, b]:

$$\sigma_s = \frac{4\pi a^2}{\left[\left(\frac{f_R}{f}\right)^2 + \delta^2\right]} \qquad (8.1.4)$$

where f_R and f are resonant and source frequency respectively, and δ is the damping constant. Figure 12a shows theoretically calculated values of scattering cross section for 3.5 kHz and 50

kHz sources. If bubble clouds are tightly packed, bubble-bubble interactions and multiple scattering will broaden the resonant peak [Vagle and Farmer, 1992].

The expression for scattering cross section in equation (8.1.4) is valid for bubble radii which are small with respect to the acoustic wavelength in the medium [Akulichev *et al*., 1986]. For our 3.5 kHz and 50 kHz acoustic sources, the acoustic wavelengths in seawater are approximately 40 cm and 3 cm respectively. The distribution of bubble sizes for the La Goleta Seep field was estimated by analyzing a video of gas bubbles rising through a grid of known dimension placed at the sea surface. This distribution of bubble sizes is shown in Figure 12b. However, distribution of seep gas bubble sizes is not necessarily homogenous throughout the offshore Coal Oil Point area.

Figure 12: (a) Calculated theoretical scattering cross section verse bubble radius for 3.5 kHz and 50 kHz sources, and (b) observed distribution of bubble radii at the surface above the Seep Tents.

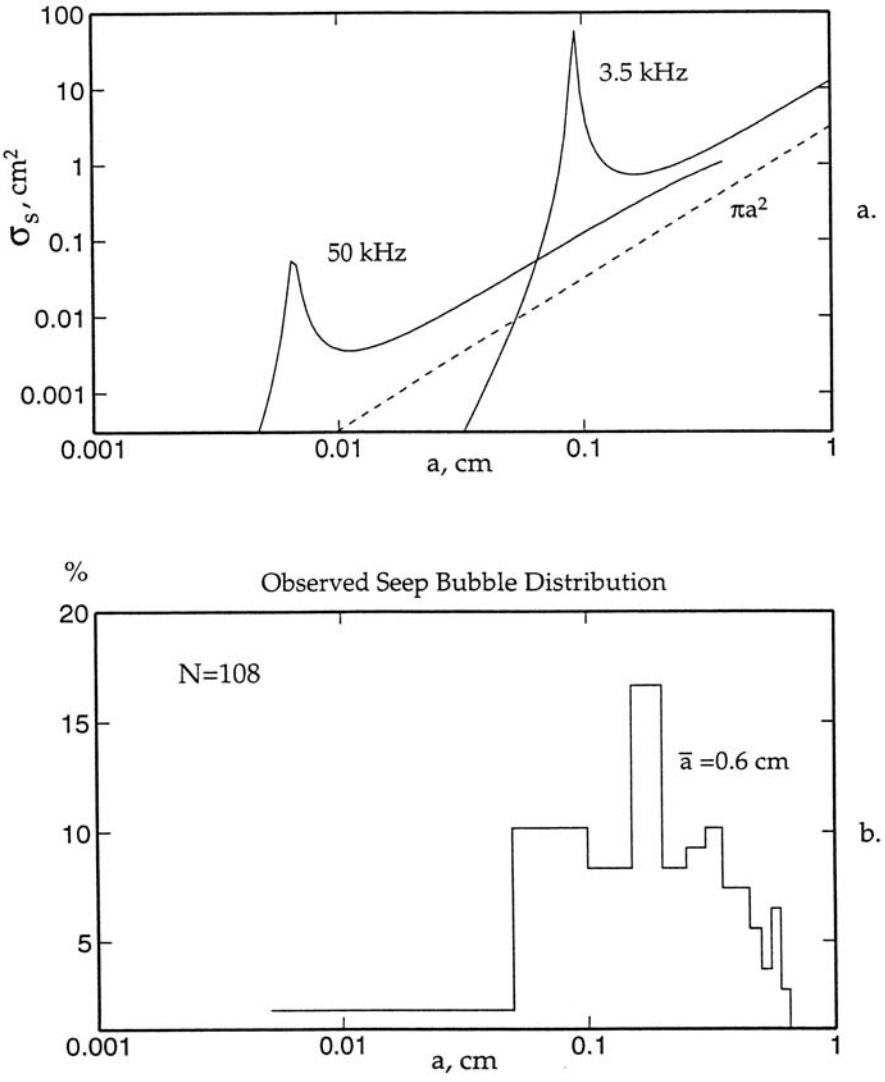

Mean bubble radii for the observed distribution of 108 bubbles was 0.6 cm. This is sufficiently small in comparison to the acoustic wavelengths used but large compared to typical bubble sizes in near surface ocean waters [Wu, 1981] arising from natural processes other than submarine gas seepage. Bubble radii decrease with depth as does the radii of the resonant peak, both due to increasing ambient pressure. Measured bubble radii presented in Figure 12b were taken at the ocean surface and the calculated theoretical curves in Figure 12a are likewise based on surface values. The theoretical calculation was also performed assuming air was the bubble gas composition, whereas the true composition of the seep gas is given in Table 1. The parameters in equation (8.1.4) are dependent on properties of the gas composition such as density and specific heat [Medwin, 1977a], but these are second order effects.

The peak of the observed bubble size distribution (Figure 12b) is well away from the theoretically calculated 50 kHz resonant peak but overlaps the 3.5 kHz peak (Figure 12a). Since our interest is in estimating volumes of gas entrained as bubbles, we are most interested in the larger radius bubbles as they contain the most volume (increasing as a^3 for spherical bubbles). However, overlap of the 3.5 kHz resonant peak shown in Figure 12a with the observed distribution of bubble sizes in Figure 12b suggests contribution by smaller radii bubbles may represent a significant portion of the sonar return for this frequency.

The integral in equation (8.1.3) implies that the solution for volume scattering cross section M_υ is non-unique and solving for the bubble size distribution based on sonar return is therefore a complicated inverse problem. The approach of Vagle and Farmer [1992] was to use multiple frequencies to derive the bubble size distribution. However, their technique was designed for measuring microbubbles ($a \leq 150$ μm) much smaller than the observed distribution of seep gas bubbles in Figure 12b. In addition, they used six frequencies as opposed to our two, and of those two the resolution and dynamic range of the (analog) 50 kHz data is limited compared to the digital 3.5 kHz data.

8.2 EMPIRICAL CALIBRATION OF SEEPAGE RATES

Faced with these difficulties and the complicated data inversion of Vagle and Farmer [1992], it was decided to attempt a simple empirical calibration of the 3.5 and 50 kHz data. To this end, sonar data was collected during a series of calibration experiments over artificial sources releasing gas at known rates. For the 3.5 kHz system an experiment was conducted off San Pedro, California in November, 1996 during which a canister of compressed nitrogen gas was connected via lengths of hose to diffusing nozzles deployed on the ocean floor in approximately 40 m water depth. Flow rates were varied for a series of sonar passes and directly measured using two flow meters, then averaged and plotted as the abscissa in Figure 13a. Although both digital and analog data were acquired during this experiment, a problem with the digitization equipment resulted in only one good digital data point being obtained.

The 50 kHz calibration was conducted separately in concert with the 50 kHz data acquisition cruises in November 1994, December 1994, August 1995, and November 1995. Each separate data point in Figure 13b was obtained during one of these cruises. The artificial source for these experiments were tanks of compressed air with a capacity of 71.4 ft^3 (2021 liters) of gas at 3300

psi pressure attached to leaking SCUBA regulators. The tanks were deployed in approximately 60 m water depth, and flow rate was inferred by measuring the initial and final tank pressure and the intervening time.

Figure 13: Empirical calibration for (a) 3.5 kHz (b) 50 kHz data.

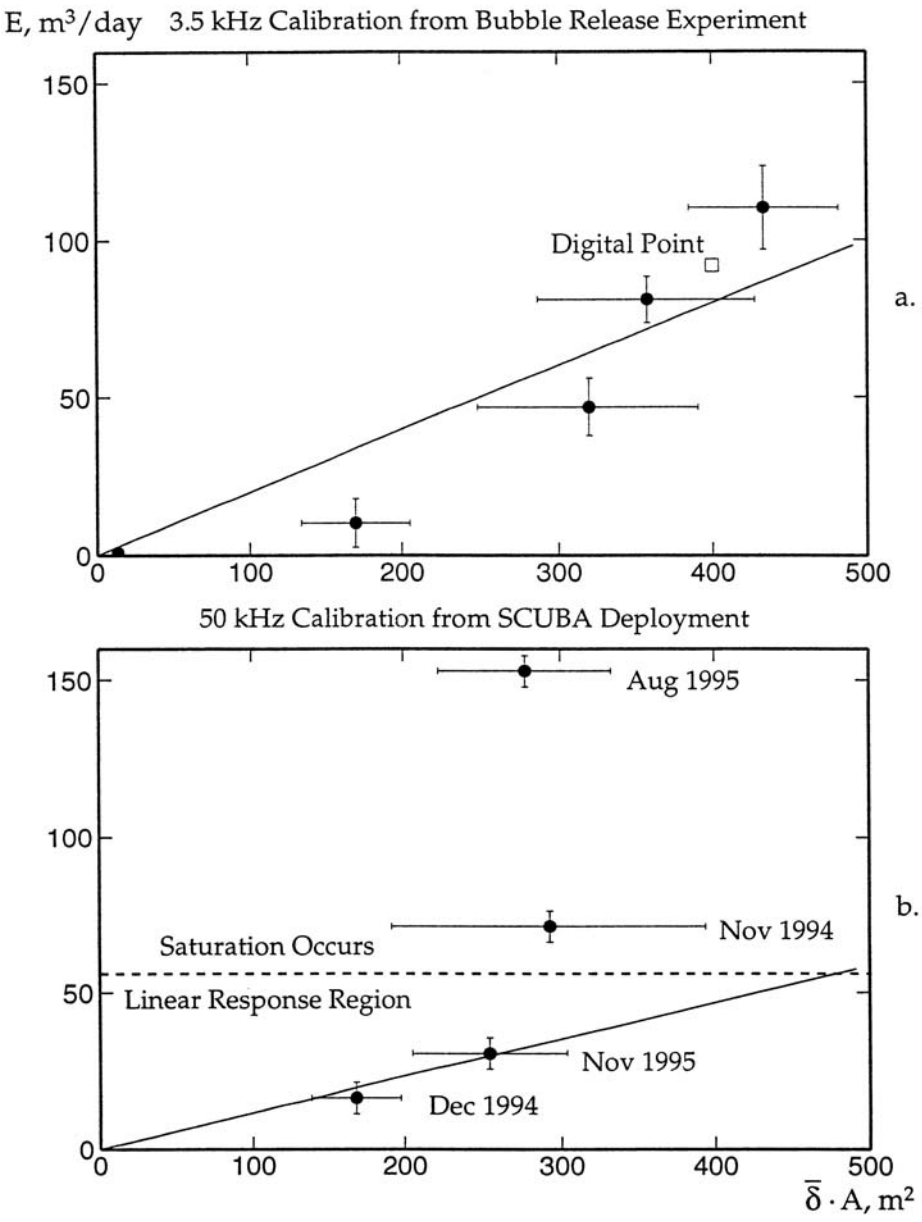

By plotting the averaged emission rates *E* against the mean values of normalized intensity profile $\overline{\delta}$ obtained over some area *A*, calibration coefficients were obtained based on empirical fits to the data. Average values $\overline{\delta} \bullet A$ verses emission rates *E* are presented in Figure 13a and b for the 3.5 kHz and 50 kHz systems respectively. The ordinate axis in each plot is the mean value of relative intensity profile δ multiplied by the survey area *A* over which the $\overline{\delta}$ profile value is averaged.

Area *A* is calculated as the product of sonar swath width with the length of the analysis window along the survey track.

An example is shown in Figure 14 for the case of a 3.5 kHz analog record. The scanned image of a plume is presented in Figure 14b for an artificial source releasing 2.45 m^3/day of gas. Each column of the 20-30 m depth analysis window is averaged to produce the corresponding δ-profile of the plume shown in Figure 14a. The mean δ value $\overline{\delta} = 0.28$ is then multiplied by the length of the analysis window (30 m) and swath width of the sonar to obtain the value of $\overline{\delta} \bullet A$ averaged for the plot in Figure 13a. Swath width of the sonar is determined at the midpoint of the 20-30 m depth window based on the beam pattern (solid angle) of the sonar and was 15 m for both the 3.5 kHz and 50 kHz systems. Length of the analysis window varied with the width of the artificial source plume, but was selected to be wide enough to encompass the whole plume profile.

Figure 14: (a) Sample intensity profile from November 1996 calibration experiment calculated from a plume above the artificial source shown in (b).

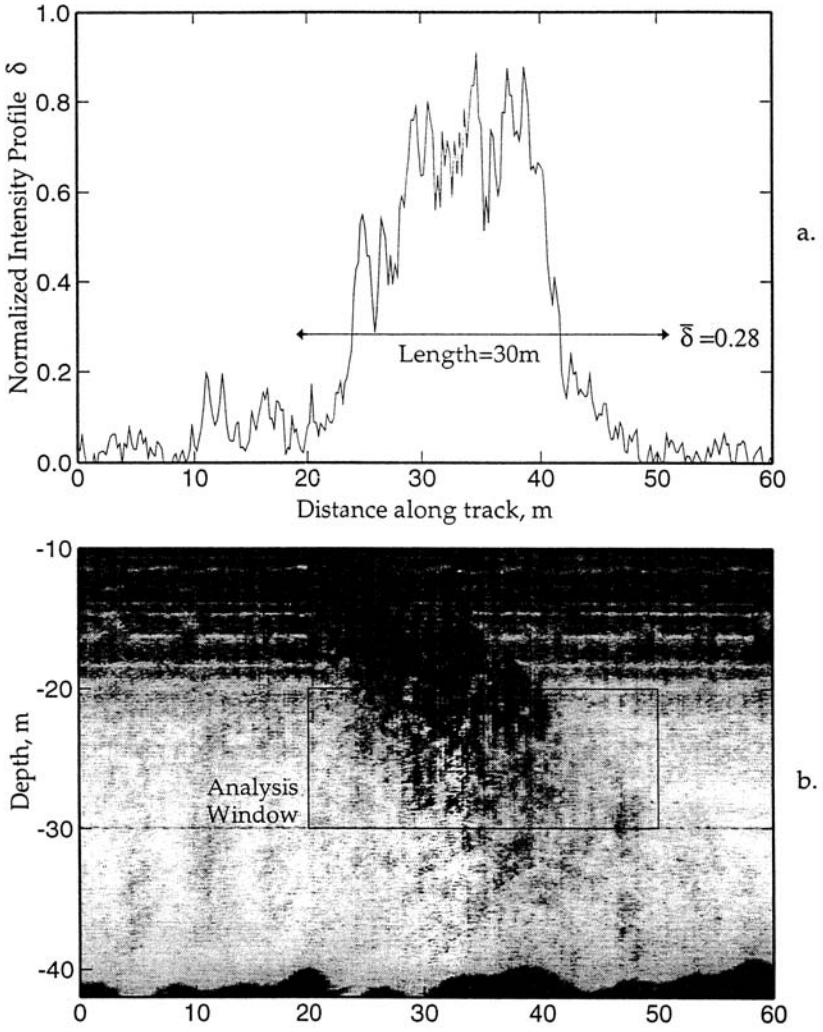

The error bars in Figure 13a and b represent the standard deviations of $\overline{\delta} \bullet A$ and emission rate E for separate sets of sonar passes. Linear least squares fits through the origin were matched to the set averages. For the 50 kHz data, the fit was only applied to the two lowest emission rates because the data appeared to saturate with increasing values of $\overline{\delta} \bullet A$. The calibration coefficients for converting relative sonar return to seep gas flux were taken as the slopes of the linear fits in Figure 13a and b for the 3.5 kHz and 50 kHz data respectively.

For the 3.5 kHz sonar, the calibration coefficient was $c_{3.5} = 0.2 \pm 0.06$ m^3/m^2.day, and for the 50 kHz system $c_{50} = 0.12 \pm 0.02$ m^3/m^2.day. Error of these coefficients is calculated (Appendix 2) from the error in the slope of the fit curve, but the actual error in the estimates may be larger due to additional sources of error unaccounted for in the calculation (see Appendix 2).

The lack of digital 3.5 kHz data from the November 1996 calibration experiment prevented the calculation of a separate digital coefficient, but the single good digital data point obtained falls close to lying on the calibration curve for the analog data in Figure 13a. Comparison of similar analog and digital profiles from July 1995 suggests the digital S profile data should by scaled upward by about 30% to correspond to the analog data. This is probably because the lack of dynamic range of the analog data causes premature saturation of the primary signal used to normalize the darkness profiles.

Although the approach for arriving at the above calibration coefficients is wholly empirical and admittedly crude, it was hoped it could provide an order of magnitude estimate of gas seep emission rates. Since the seep distributions mapped in Figure 5, Figure 8, Figure 10 and Figure 11 plot the intensity distributions greater than 0.1 $\overline{\delta}$ for analog data (both 3.5 and 50 kHz) and 0.05 $\overline{\delta}$ for the digital 3.5 kHz data, these levels correspond to 20 ± 6 liters/m^2•day, 12 ± 2 liters/m^2• day, and 13 ± 4 liters/m^2•day respectively. We can also add additional contours and re-plot these distributions in terms of the calibrated seep flux levels. This is done for the August 1996 3.5 kHz digital data (Figure 15), July and September 1995 3.5 kHz analog and digital data (Figure 16), and 1994-1995 50 kHz analog data (Figure 17) respectively.

Figure 15: Calibrated map of flow rate for August 1996 digital 3.5 kHz surveys.

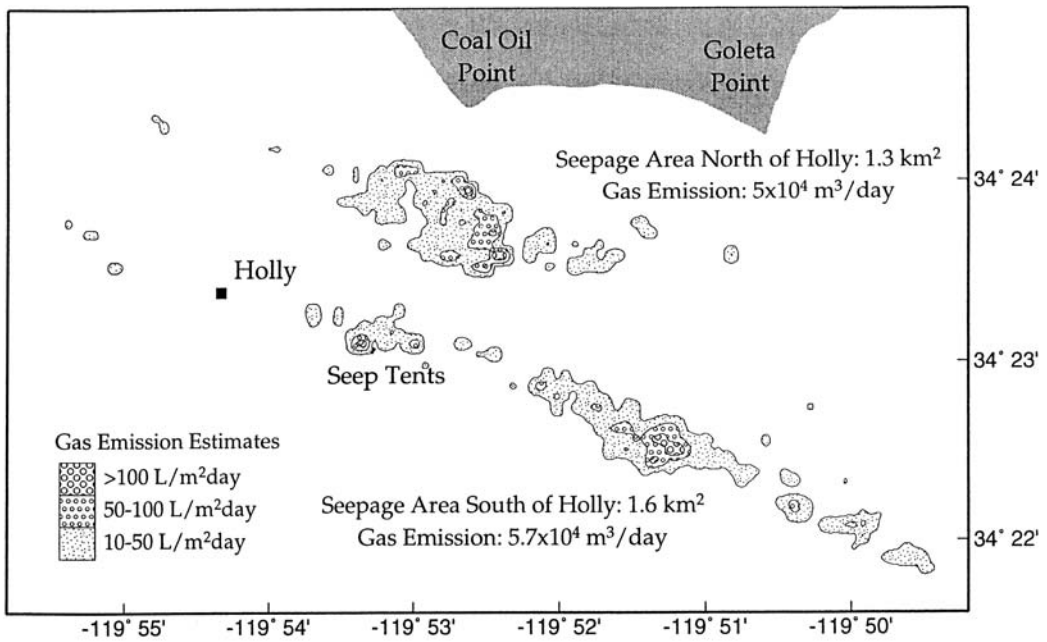

Figure 16: Calibrated map of flow rate for July and September 1995 analog and digital 3.5 kHz data.

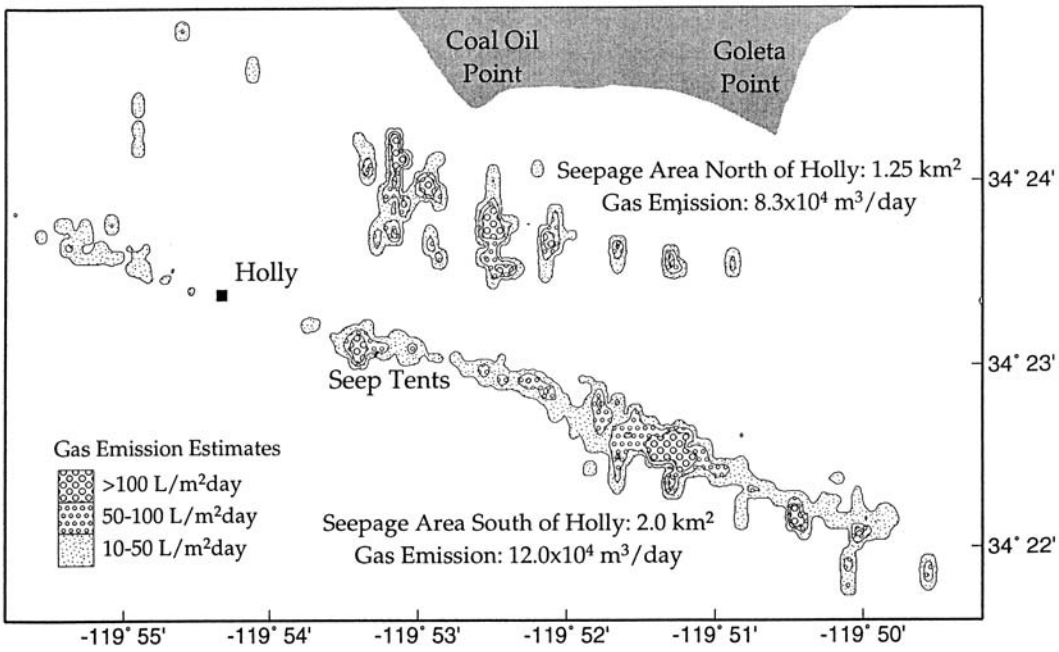

Figure 17: Calibrated map of flow rate for 50 kHz surveys.

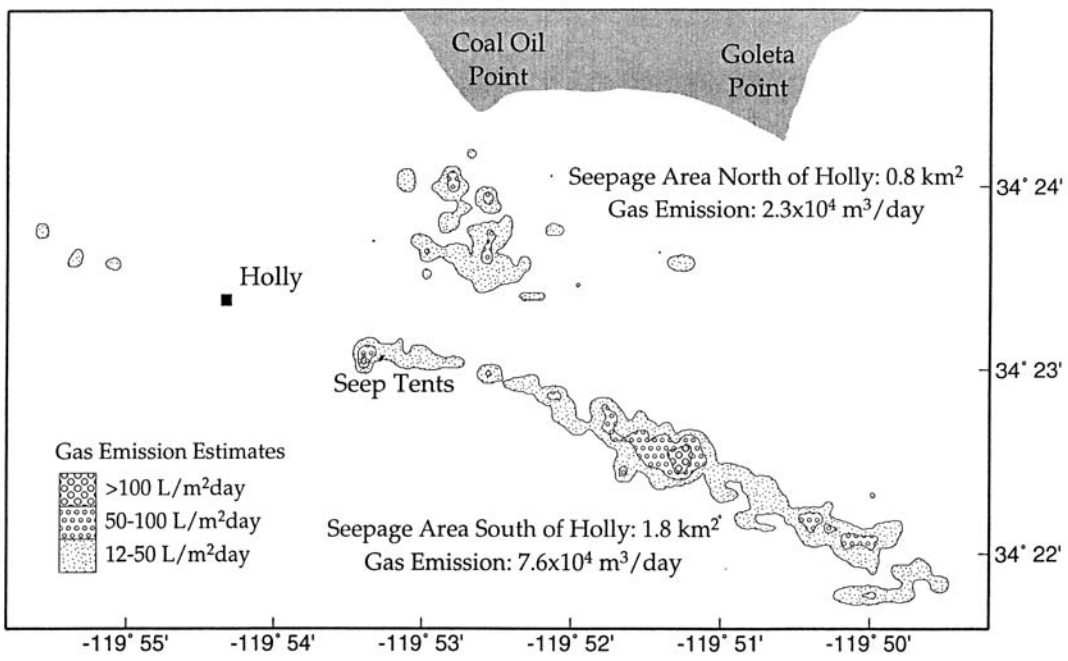

8.3 EMISSION ESTIMATES

The total emission of seep gas from offshore Coal Oil Point for each survey can be estimated by summing the values over the gridded data set and multiplying by the appropriate calibration coefficient:

$$E_t = c \cdot \sum \bar{\delta} \cdot A \qquad (8.3.1)$$

The area of each grid node was 100 by 100 m, or 10^4 m^2, and only δ values greater than 0.1 or 0.05 for analog and digital data respectively were included for the estimate. The total emission estimates (Table 2) are $10.7 \pm 3 \times 10^4$ m^3/day of gas for August 1996, $20.3 \pm 6 \times 10^4$ m^3/day for July and September 1995, and $9.9 \pm 2 \times 10^4$ m^3/day for the 50 kHz data spanning 1994 and 1995.

Table 2: SUMMARY OF EMISSION ESTIMATES FOR THE COAL OIL POINT AREA

	Seep Gas, m^3/day	Methane metric tons/day	non-methane hydrocarbons metric tons/day	liquid petroleum liters/day	ROG evaporates from oil metric tons/day
Fischer, 1973:					
13 km^2 of Holly	$5.1x10^4$	22.6	7.5	4590	2.0
50 kHz surveys:					
North of Holly	$2.3x10^4$	10.2	3.4	2070	0.92
South of Holly	$7.6x10^4$	33.7	11.1	6840	3.1
Total	$9.9x10^4$	48.8	14.5	8910	4.0
July-Sept 1995:					
***13 km^2 of Holly**	$2.3x10^4$	10.2	3.4	2070	0.92
North of Holly	$8.3x10^4$	36.8	12.2	7470	3.3
South of Holly	$12.0x10^4$	53.2	17.6	10,800	4.8
Total	$20.3x10^4$	90	29.8	18,270	8.1
August 1996:					
North of Holly	$5x10^4$	22.2	7.3	4500	2.0
South of Holly	$5.7x10^4$	25.3	8.4	5130	2.3
Total	$10.7x10^4$	47.5	15.7	9630	4.3

*Only for July 1995.

The distributions of emissions plotted in Figures 15, 16, and 17 demonstrate that volumetric flow from seepage in the offshore Coal Oil Point area is greatest above the culminations along the South Ellwood Anticline axis (Figure 3) and also due south of Coal Oil Point along what may be the trace of the fault described in Section 5.1 noted by Fischer [1977]. Comparison of flow rates for the different surveys seem to indicate flow rates are higher by a factor of two in July and September, 1995 compared with August 1996 and the 50 kHz data from 1994 and 1995. However, it is possible that the difference between these estimates arises from errors. Although the estimated error in seep flux calculated in Appendix 2 is only 20-30%, perhaps it should be revised upwards to 50% in order to encompass the observed range of estimates and account for additional errors not accounted for in the calculation (see Appendix 2).

It is certainly likely that there is some fluctuation in seepage rates, but our ability to accurately observe such fluctuations probably depends on their scale in both time and in volume. For example, the decrease in areal cover of seepage in the 13 km^2 area around Holly over a 20 year time period presented in Figure 7 would be accompanied by a concomitant decrease in seepage calculated in Figure 18. Using the arbitrary 50% error suggested above, the estimated change in gaseous emission (Table 2) for this area declined from $5.1 \pm 2.5 \times 10^4$ m^3/day in 1973 to $2.3 \pm 1.2 \times 10^4$ m^3/day in 1995.

If the individual estimates calculated from Figures 15, 16, and 17 are sufficiently accurate and precise, this represents a significant variation in seep flux on a short term (1 year) time scale as well. Neglecting the 50 kHz data which may differ due to its different frequency response, the apparent reduction of seepage between July - September 1995 and August 1996 could represent

part of a longer term trend of seep decline suggested by Figure 18. On the other hand, it might result from natural cyclic variations. The total seep emission for August 1996 (Figure 15) is actually larger than the 50 kHz estimate for 1994 and 1995 (Figure 17) which contradicts a hypothesis of decreasing rates of seepage over time. However, if Platform Holly is used to reference a demarcation line separating the further offshore seeps of the South Ellwood Seepage Trend to the south from the more inshore Goleta Seepage Trend to the north, spatial variations in seep emission are observed as well rather than a coherent variation for the entire offshore area.

South of Holly navigational coverage extending to the southeast along the South Ellwood Anticline axis is sufficiently robust to allow a good comparison of seep distributions from the different surveys. The seep distribution mapped south of Holly from the 50 kHz data (Figure 17) presents a larger areal extent of seepage and higher rate of gas emission than the August 1996 data (Figure 15). However, north of Holly the seepage covers less area and has a lower emission volume. It should be noted again, however, that differences in the frequency response between the 50 kHz and 3.5 kHz data may prevent a direct comparison.

Comparison between emission volume estimates from 3.5 kHz data from August 1996 (Figure 15) and July and September 1995 (Figure 16) are consistently different by a factor of two both north and south of Platform Holly. South of Holly the decrease in seep area along the South Ellwood Anticline may partly explain the lower emission in August 1996, but flow rates are also lower. In fact, north of Holly seepage covers a larger area in August 1996 but emission is still lower, although the dissimilarity in navigational cover makes this interpretation more problematic. However, it appears seepage varies independently both spatially and volumetrically.

Causes other than error which could adequately explain the observed short term variations in seep distributions and fluctuations in emission rates remain elusive. Whether the apparent variability in seep distribution and emission rate fluctuate randomly or cyclically over time, or rather are part of a longer term monotonically decreasing trend is unclear. A long term trend producing the alteration of seepage around Holly displayed in Figure 18 suggests a monotonic decrease since this area is consistently barren of seepage in all our surveys.

Figure 18: Comparison of gas emission for (a) 1973 3.5 kHz data from Fischer and (b) July 1995 3.5 kHz analog data.

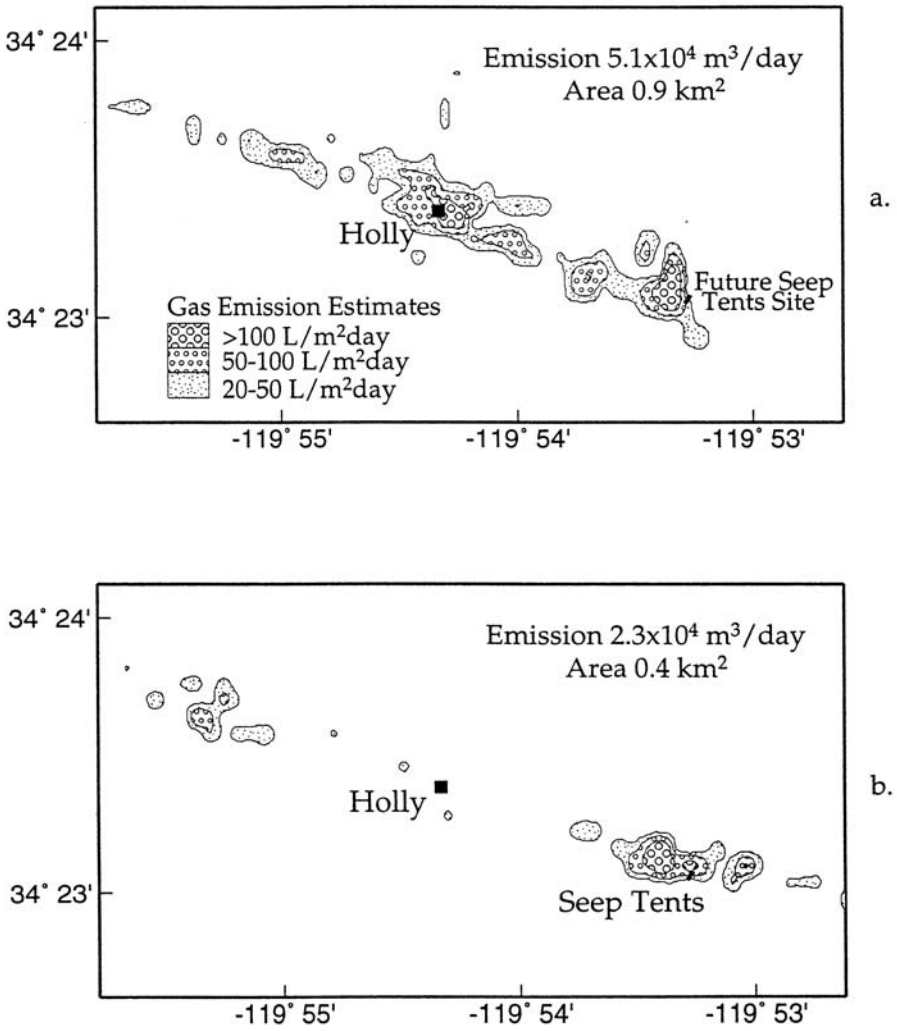

Time series of average monthly emission volumes collected at the Seep Tents presented in Figure 19a also show a long term decline in emission rate. However, there are again shorter term fluctuations within this trend which defy an easy interpretation. The initial rate of gas collection at the Seep Tents following their installation in 1982 was 1,050,000 ft^3 (30,000 m^3) of gas per day [Guthrie and Rowley, 1983]. Subsequent production increased due to the addition of flaps to the Seep Tents structure, causing the increase observed in 1987 (Figure 19a) [J. S. Hornafius, pers. comm., 1996]. Average production from 1983 to 1990 was 1,270,000 ft^3/day (36,000 m^3/day) [Hoviand *et al*., 1993].

Figure 19: (a) Monthly averages of production volumes of seep gas at the Seep Tents and (b) annual oil production from Platform Holly.

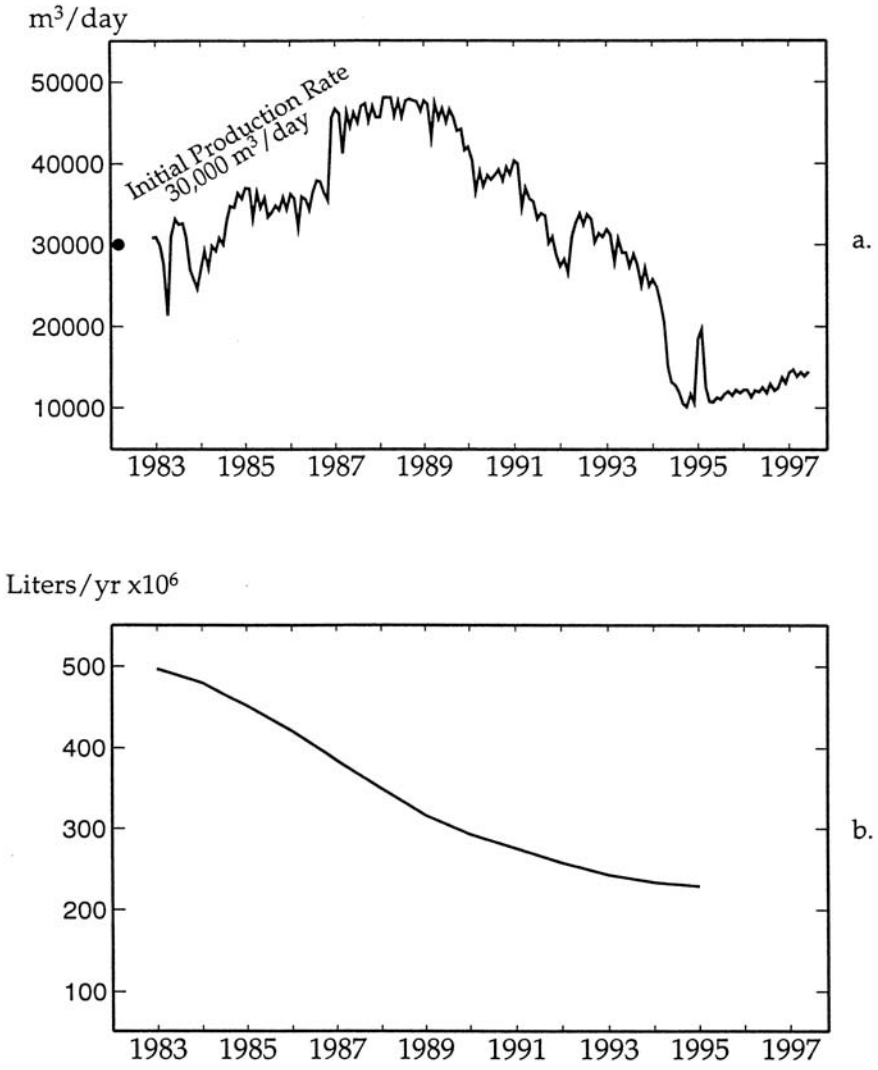

Around 1989-1990 a gradual decrease in seep emissions began (Figure 19a) which by 1994 had declined to about half of the peak production during 1987-1989. The sharp roll-off in Figure 19a after 1994 was caused by a mechanical failure of the line from one of the Seep Tents which was subsequently repaired but again failed, causing the spike in the time series in 1995 [J. S. Hornafius, pers. comm., 1996]. The mechanical problems affecting the Seep Tents prevent comparisons at the times of our surveys in 1995 and 1996. The second order fluctuations during the overall decline between 1989 and 1994, however, are not explained by mechanical factors.

Oil production is a reasonable mechanism for producing the progressive long term declines in seepage illustrated by Figure 18 and Figure 19a. From 1983 to 1995, annual oil production from Holly gradually decreased from 500 $x10^6$ liters/year to about 200 $x10^6$ liters/year (Figure 19b) with corresponding gas production of 300 to 500 ft^3/barrel (50 to 90 liters of gas/liter of oil) [J. S. Hornafius, pers. comm., 1996]. Figure 19b is a smooth curve, lacking sharp spikes in production

that might account for the dips in seepage in 1990 and 1992 in Figure 19a. Furthermore, gas re-injection, which might also effect seepage rates, was not practiced at this time.

It is interesting to speculate on other possible causes which could account for the second order variations which accompany the overall trend of declining seep emission demonstrated by Figure 18 and Figure 19a. Short period tidal fluctuations might by partially responsible. Long period cyclic variations could include seasonal affects associated with gravity drive from groundwater reservoir pressure or water temperature altering oil viscosity and methane gas solubility. Such mechanisms might also account for the observed short term variations between Figures 15, 16, and 17. The longer term trend of a 50% reduction in seepage within 13 km^2 of Holly over a 20 year period (Figure 18) and the 50% decline at the Seep Tents over a 5 year period (Figure 19a) probably arises due to oil production, and suggests a total decline of gaseous emission on the order of 50,000±20,000 m^3/day since 1973!

9.1 DISCUSSION

The data presented here demonstrate both spatial and temporal variation in the distribution and emissions of natural gaseous marine hydrocarbon seepage offshore of Coal Oil Point. The dominant spatial constraint on seep distribution is structural control as addressed in Section 5.1. The distribution of offshore seepage mapped from the August 1996 3.5 kHz data with respect to the various structural trends is presented in Figure 20. A north-south cross section of the subsurface geology offshore Coal Oil Point interpreted from well data after Bartsch *et al*. [1996] is presented in Figure 21a. The elongated linear seep trend furthest offshore is tightly confined to the South Ellwood Anticline Axis with the points of most intense seepage at structural culminations where relief of the Sisquoc-Monterey contact is more shallow. This is illustrated in the interpreted geologic cross section along the axial trend of the South Ellwood Anticline (Figure 21b, after [Bartsch *et al*., 1996]).

Figure 20: Contour plot of thickness (in meters) of Quaternary sediment overburden, geologic structure, and August 1996 seep distribution offshore of Coal Oil Point.

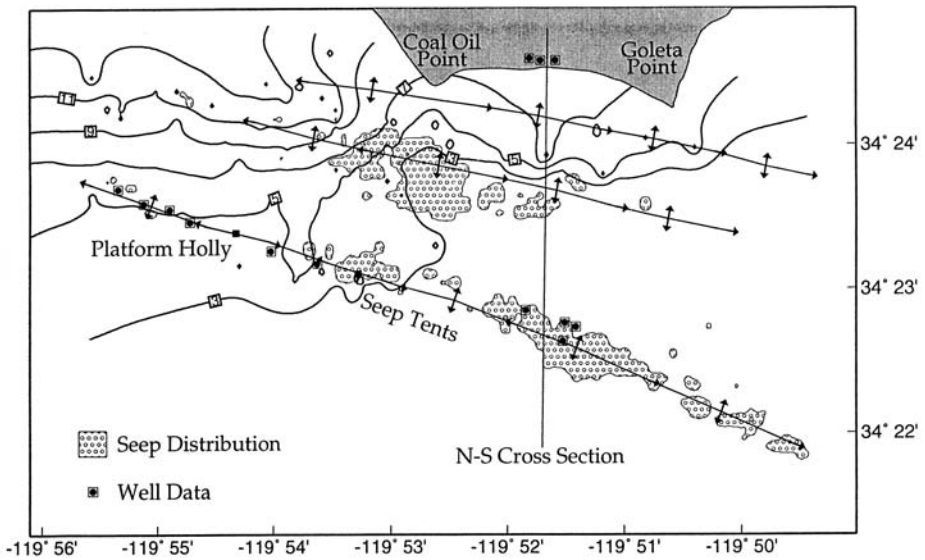

Figure 21: Stylized interpretation of subsurface geologic structure offshore of Coal Oil Point after [Bartsch, et al., 1996] based on seismic and well-hole data for (a) the N-S line in Figure 21 and (b) along the axial surface of the South Ellwood Anticline.

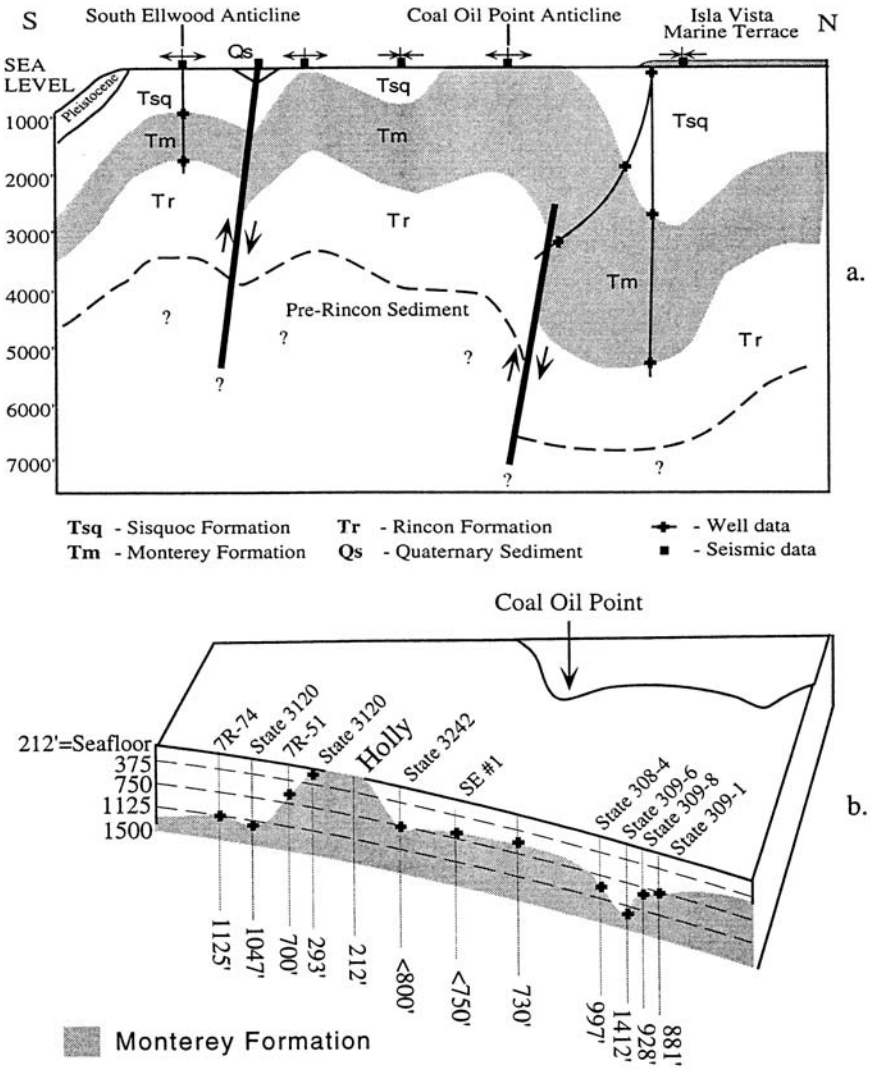

The further inshore seepage area due south of Coal Oil Point also coincides with the structural culmination along an anticline axis but is more disperse, possibly due to fault splays at the intersection of cross faults with the anticline axis and synclinal limbs [Bartsch *et al*., 1996]. Reverse faulting such as that observed for the South Ellwood Offshore oil field [Division of Oil and Gas, 1991] is perceived to be associated with the tight compressive folding offshore (Figure 21a). Such faults could provide migration conduits for seepage in addition to the dense network of crestal fractures in the anticline axes inferred by Fischer and Stevenson [1973] from the absence of seismic reflections.

Thickness of the overburden of unconsolidated sediment has also been proposed to control seepage distribution [Fischer and Stevenson, 1973; Fischer, 1977]. To examine the correlation between seep locations and sediment overburden, an isopach of the Quaternary sediment thickness produced from 3.5 kHz data is also presented in Figure 20. Cover by the Quaternary sediment becomes thin or absent towards the southeast portion of the map, but this thin sediment veneer is fairly uniform throughout a region of variable seep distribution. This suggests structural control is more likely the dominant constraint on seep configuration, although thinning of the Quaternary cover may reflect where sediment overburden is truncated over structural highs which correspond to seepage.

Comparison of the seep distributions mapped from different surveys reveals variations in seepage patterns. Some minor variations in position on the order of 30 m (see Section 7) may be due to changes in the direction and velocity of ocean currents which could shift the position of seep gas bubbles in the water column relative to their seafloor source. In addition, errors in the mapped seep distribution may result as an artifact of different navigational coverage. However, some changes in seep distribution patterns are likely to be real. A case in point is the disappearance of seepage around Platform Holly between 1973 and 1995 illustrated by Figure 7. Seepage at Holly was prolific in 1973, but while navigational cover of this area is robust for all surveys from 1994 through 1996 (Figures 5, 8, and 10), seepage is consistently absent (Figure 11), suggesting a long term disappearance of the seeps at this site.

Changes in seep distribution could result from drying up of seep source hydrocarbons or changes in subsurface migration pathways acting as seepage conduits. Creation of fault-induced fracture pathways associated with seismic activity, exposure of new seep vents through erosion, or sealing of active vents by viscous residual tar are all possible mechanisms which could affect seep distribution. However, the spatial coincidence between the location of Platform Holly and the disappearance of seepage between 1973 and 1994 suggests that the anthropogenic effect of oil production is probably largely responsible for this disappearance.

Oil production has been proposed as a mechanism for reducing seepage as the reservoir of source hydrocarbons is drawn down by producing wells [Landes, 1973; Kvenholden and Harbaugh, 1983]. Draw down of reservoir hydrocarbons could lead to reduction of reservoir pressure which could cause declines in seepage rates since velocity of fluid flow in a porous medium is proportional to the pressure gradient and inversely proportional to fluid viscosity from Darcy's Law [Craft and Hawkins, 1959]. Reduction of reservoir pressure is proposed as a factor in reducing seepage in the vicinity of Coal Oil Point [Fischer and Stevenson, 1973; Fischer 1977], but production could also reduce seep emissions by diminishing the quantity of hydrocarbons available for seepage. Either of these mechanisms could account for decrease in areal coverage of seepage and also decline in emission volumes.

Figure 22a presents reservoir pressure measurements corrected to a common depth of 3881 ft (1180 m) subsea for various sites around Platform Holly shown in map view in Figure 22b. Figure 22a shows a decline in reservoir pressure over time beginning approximately in 1981. The initial pressure is only slightly above hydrostatic, and pressure within the reservoir drops below hydrostatic fairly early in the production history. If the pressure gradient in the reservoir is not

super-hydrostatic, pressure should not be sufficient to drive the vertical migration of seepage. Therefore, initial declines in reservoir pressure below hydrostatic may have reduced pressure driven seepage in the spatially restricted area around Holly.

Figure 22: (a) Reservoir pressure values in the Monterey Formation reservoir exhibit spatial dependence on well locations relative to Holly shown in (b) and decline over time with production.

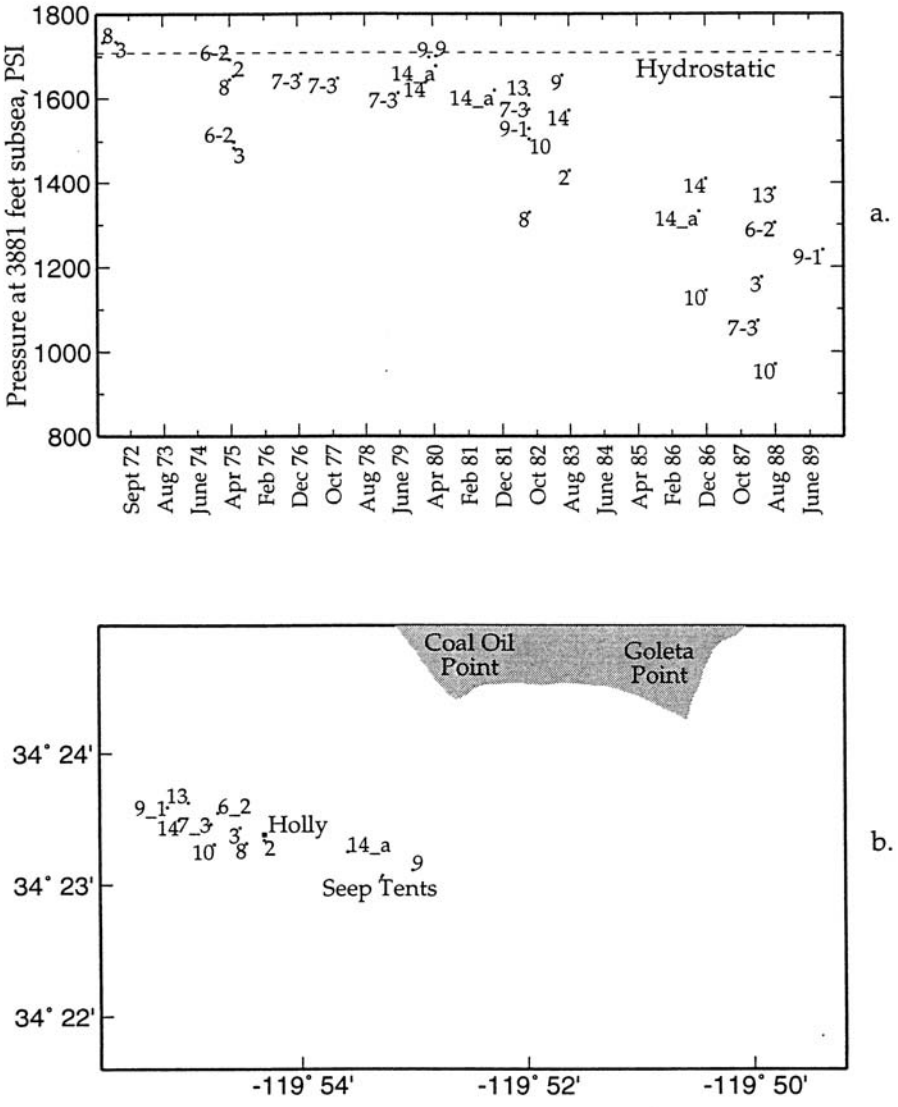

Buoyancy of gaseous phase hydrocarbons dominate fluid potential gradients in the shallow subsurface [Clarke and Cleverly, 1991] and may be another appropriate mechanism for driving the seepage offshore Coal Oil Point given the gaseous nature of these seep trends. Buoyancy of the gas phase could also transport oil through the Sisquoc cap rock from the underlying Monterey Formation reservoir. The velocity of buoyant transport would be essentially constant if not coupled with pressure drive, and seep flux would then depend only on the volume of hydrocarbons undergoing transport. The diversion of migrating hydrocarbons to production could reduce available seep volumes, thus possibly accounting for some of the disappearance of

seepage around Holly and reduction in emissions at the Seep Tents.

Gas production from the Monterey Formation Reservoir beneath Holly commenced in 1977 prior to which gas was re-injected. Subsequently this practice ceased which may partially explain the declines in reservoir pressure beginning in 1981 (Figure 22a). Analysis of $\delta^{13}C$ of seep gas collected at the Seep Tents indicates it is compositionally consistent with the produced gas from the Monterey Formation reservoir [J. S. Hornafius, pers. comm., 1996]. The gas to oil production ratio from the reservoir gradually increased over time from 300 to 500 ft^3/barrel (50 to 90 liters of gas/liter of oil) due to the exsolution of gas with declining reservoir pressure [J. S. Hornafius, pers. comm., 1996]. Therefore a significant quantity of gas was removed from the reservoir in conjunction with oil production (Figure 19b). If the seep gas originated in the produced Monterey reservoirs, this represents a significant removal of gaseous hydrocarbons available for seepage.

The decline in seepage volumes at the Seep Tents beginning in 1989 (Figure 19a) also demonstrates the trend of decreasing seepage which may be the result of ongoing production drawing down the reservoir hydrocarbons and reducing reservoir pressure. The period of steady seep emissions at the Seep Tents preceding the gradual decline which began in 1989 might be explained as a lag time. Seepage could be decreasing progressively outward away from Platform Holly as production is pursued further and further afield from Holly's central location. The disappearance of seepage immediately adjacent to Holly (Figure 7) supports this hypothesis.

Declines in reservoir pressure also appear to exhibit a spatial correlation with the distance to Holly based on the data in Figure 22. This reduction in the pressure drive for seepage, as proposed by Fischer [1977], would support a progressive decrease in seepage outward away from Holly. The changes in seep distribution are accompanied by simultaneous changes in gas emission. The disappearance of seepage from around Platform Holly caused an estimated reduction in seepage of $2.8 \pm 1.4 \times 10^4$ m^3/day between 1973 and 1995 (Table 2, Figure 18), while emission similarly declined at the Seep Tents by 2.5×10^4 m^3/day between 1989 and 1995 (Figure 19a).

In addition to the anthropogenic effects of oil production, various other mechanisms could account for fluctuations in seep emission. Seismic activity is no doubt important, and could cause episodic seepage events such as that observed by Field and Jennings [1987]. However, there is only anecdotal evidence (e.g.- [Fischer, 1977]) of seepage events associated with seismic activity in the Coal Oil Point Area. Storm surges and mud diapirism could trigger another type of episodic seepage event associated with degassing from sediments [Hovland *et al*., 1993], but this is unlikely for Coal Oil Point where the seep gas migrates from a deep reservoir rather than occurring in shallow sediments.

Tidal fluctuations might cause periodic oscillations in seepage rates, as observed by Mikolaj and Ampaya [1973] for the nearshore Isla Vista oil seeps, but although gas seep emission might have been higher at low tide in Figure 9, this was not clear-cut. Gas collection at the Seep Tents (Figure 19a) does not appear to exhibit periodic tidal cycles although spectral analysis of gas production records from the Seep Tents could not be used to determine a dependence on tides since the daily averages of gas volume would alias the shorter tidal periods and tidal pumping of

gas already trapped by the Seep Tents structure might be incorrectly interpreted as variation in emissions from the seafloor seep source. In addition, interpretation of short term changes in Figure 19a is complicated by mechanical factors (see Section 8.3).

If cyclic seasonal variations or spiky episodic events are visible within the Seep Tents production record (Figure 19a) they are a second order effect in comparison to the dominant trend of declining seep emission. Seasonal changes in groundwater reservoir pressure associated with gravity-driven pumping by meteoric waters which oscillate with drought cycles could conceivably affect seepage rates. However, Monterey formation waters have sea water salinities [J. R. Boles, pers. comm., 1997], which suggests a lack of mixing with meteoric recharge water, thus reducing the likelihood that gravity flow affects seepage significantly. Seasonal changes in water temperature changing oil viscosity or methane solubility could influence oil and gas seepage rates respectively, but evidence is lacking for seasonal variations in seepage, although it is a possible mechanism for varying seepage rates.

The anthropogenic effect of oil production drawing down hydrocarbons within the reservoir seems to be the most likely candidate for producing the observed long term declines in seep emissions demonstrated by Figure 18 and Figure 19a. Ostensibly this long term trend should continue into the future if production continues. The data presented here offers a baseline for future comparison. Current estimates of the gaseous seep emissions (Table 2) for the Coal Oil Point area range from $9.9 \pm 5.0 \times 10^4$ m^3 of gas per day for the 50 kHz data (Figure 17) to $20.3 \pm 10.0 \times 10^4$ m^3 of gas per day for 3.5 kHz data from July-September 1995 (Figure 15) based on an empirical calibration of relative sonar return with an arbitrary 50% error (see Section 8.3).

Some variation in these estimates may be due to error (see Appendix 2). However, it is likely that additional variations in both spatial distribution of seepage and volume emission occur at time scales other than that of the observed long term decline. Unfortunately, causes for these shorter term variations are not as obvious. If the data in Figures 15, 16, and 17 are accurate we are seeing changes in emission by a factor of two over a one year period. This represents a significant fluctuation in seepage.

The better constrained emission data from the Seep Tents (Figure 19a) demonstrates a 50% reduction in seepage but on a more reasonable five year time span. However, this is emission from a point source, and the decrease in area (about 20% along the South Ellwood Anticline Axis South of Holly) between July-September 1995 (Figure 16) and August 1996 (Figure 15) could partially account for a similar reduction in flux on a shorter one year time scale for the entire offshore area.

9.2 SEEP METHANE FLUX

Annual flux of methane based on the above estimates of seep gas flux would range from about $2.4 \pm 1.2 \times 10^{10}$ to $5.0 \pm 2.5 \times 10^{10}$ g/year where we have incorporated the arbitrary 50% error assigned in Section 8.3. This assumes a seep gas composition consistent with Table 1 (90% methane by volume). No effort is made to account for dissolution of methane within the water column which could represent a significant sink for the methane gas before it reaches the

atmosphere [Cynar and Yayanos, 1992]. It is assumed that emission of liquid oil which accompanies the gaseous seepage forms rims around the gas bubbles which inhibit dissolution by creating a double boundary layer. Methane solubility in water is also temperature dependent, but this is a fairly insignificant effect, decreasing about 20% from 10° C to 20° C [Lange *et al*., 1941].

The above estimate of methane flux from the Coal Oil Point Seeps is insignificant in comparison to an estimated total annual methane flux of $540x10^{12}$ g/year [Cicerone and Oremland, 1988]. Therefore, the significance of natural seepage as a source of methane in the global budget is dependent on how widespread seeps are. Evidence of gas in marine sediments [Judd and Hovland, 1992] suggests submarine seepage of methane may be an ubiquitous occurrence on the worlds continental shelves [Hovland and Judd, 1988]. However, seepage rates as high as those observed for the Coal Oil Point area are likely to be uncommon [Hovland *et al*., 1993].

Hovland *et al.* [1993] estimated worldwide seepage contributed from 8 $xl0^{12}$ to 65 x 10^{12} g of methane annually to the global budget, which represents a significant input. To arrive at this estimate, Hovland *et al*. [1993] assumed natural gas seeps are log-normally distributed. Wilson *et al*. [1974] previously made this assumption for liquid petroleum seeps. The assumption is based on the fact that quantities such as oil field sizes, basin hydrocarbon reserves, and well-production rates are log-normally distributed, and seepage rates should be functions of many of the same parameters. However, Kvenholden and Harbaugh [1983] questioned this conclusion on the grounds that hydrocarbon accumulations smaller than producing fields could still account for seepage.

To examine the size distribution of gas seeps in the Coal Oil Point area, histograms of gas flux for each grid node (l00 x 100 m) were obtained for the 50 kHz data, August 1996 3.5 kHz data, and July and September 1995 3.5 kHz data. These histograms are presented in Figure 22a. The bins on the histograms were only calculated for values of gas flux above the background level (approximately 10 liter/m^2 day). In Figure 21b, a log-log plot of gas flux values verses cumulative percent of the gas flux distribution is presented. Such a plot should yield a straight line for log-normally distributed data [Hovland *et al*., 1993]. Each dataset fits a straight line reasonably well, but exhibits some curvature that may suggest the data is not lognormal, or may arise due to errors in the measurement technique. The fact that the distribution of emission for the July and September 1995 3.5 kHz data levels off at the higher flow rates (Figure 23) may suggest saturation of the analog portion of the data, and therefore imply errors in the emission estimate from this data set.

Figure 23: (a) Distribution of emission rate per grid node for each dataset and (b) log-log plot of emission vs. cumulative percent.

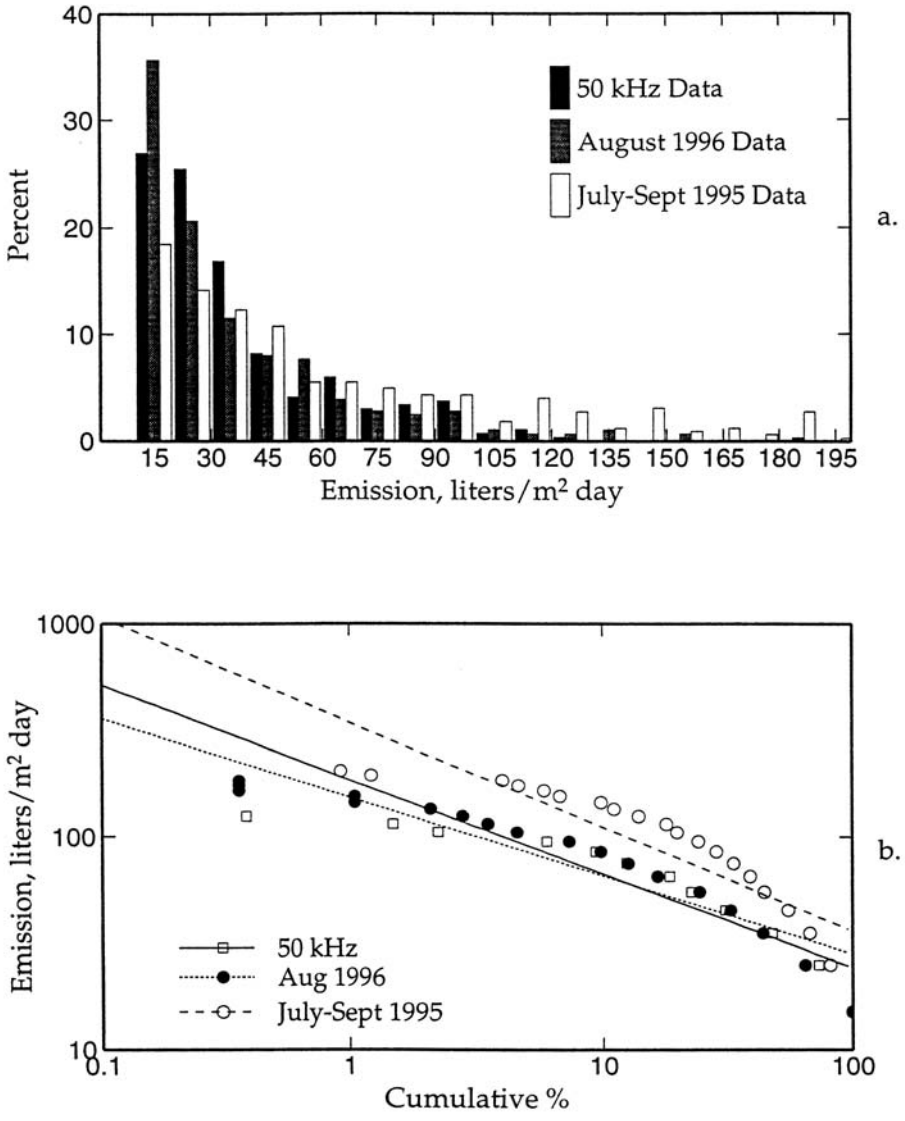

9.3 SEEPAGE OF LIQUID PETROLEUM

Seepage of liquid petroleum also accompanies the flux of gas from the Coal Oil Point Seeps. The rims of oil film which surround the venting seep gas bubbles at the seafloor are buoyed upward through the water column to the surface resulting in slicks. Oil seepage accompanying gas flow from the outer seep trends was estimated to be about 80 barrels/day (12,800 liters/day) [Clester *et al*., 1996] based on an oil gas ratio of 90 cm^3 of oil per m^3 of gas [Clester, pers. comm., 1996]. Given the estimates for gas emission above, corresponding seepage of oil (Table 2) would range from about 9000 to 18,000 liters (55 to 110 barrels) per day with an arbitrary 50% error (Section 8.3). This is in addition to the 50 to 70 barrels per day (8000 to 11,000 liter/day) estimated by

Allen *et al*. [1970] for the nearshore oil seeps. Total seepage of liquid petroleum for the entire offshore area could thus range from about 105 to 180 barrels (17,000 to 29,000 liters) per day. This range encompasses the estimate of 150 barrels per day (24,000 liters/day) of Clester *et al*. [1996] and is within the span of the estimate by Fischer [1977] of 25 to 400 barrels (4000 to 64,000 liters) per day.

The magnitudes of the above estimates demonstrate the prolific nature of natural seepage offshore Coal Oil Point and illustrate the potential of significant contributions from seepage to the marine environment. Previous work has already shown this is true on a global scale. For example, previous estimates of the total mass flux of liquid petroleum into the marine environment range from 0.25 million metric tons per year [Kvenholden and Harbaugh, 1983] to 0.6 million metric tons per year [Wilson *et al*., 1974]. This represents up to 10% of the input from both natural and anthropogenic sources of petroleum, whose total input to the marine environment is roughly 6 million metric tons per year [Kvenholden and Harbaugh, 1983].

9.4 SEEP FLUX OF ROG'S

Reactive organic gases (ROG's) are also emitted by the Coal Oil Point seeps. These include all chain hydrocarbons higher than methane and ethane. ROG's are of concern for issues of air quality because they are precursors to smog forming ozone. Approximately 150 g of non-methane hydrocarbons are emitted for each m^3 of seep gas based on the gas composition in Table 1. Using the above estimates of seep gas emission (Table 2), flux of non-methane hydrocarbons from the gaseous component of seepage offshore of Coal Oil Point contributes 15 to 30 metric tons per day to the local atmosphere, plus or minus 50%.

In addition, evaporation of volatiles from the surface slicks of liquid petroleum introduces additional ROG's to the atmosphere. The seep oil which forms the surface slicks has about 10 API Gravity and is composed (by weight) of 30% aromatic compounds, 27% saturates, 26% NSO compounds, and 20% asphaltic compounds [J. S. Hornafius, pers. comm., 1996]. The saturated and aromatic compounds (about 50% of the seep oil) evaporate whereas the nonvolatile NSO and asphaltic compounds are left as residual tar. The emission of ROG's due to evaporation from the surface slicks is approximately 444 g of ROG's per liter of oil. This represents a flux from 4.0 to 8.0 (± 50%) metric tons per day.

The sum of ROG emissions estimated from both gaseous and liquid components of seepage is 20 to 40 (± 50%) metric tons per day. This is within the range of the estimate of Saxena and Oliver [1984] (16.2 to 137 metric tons per day) which included *all* Santa Barbara Channel seeps (not just those at Coal Oil Point). This estimate represents a significant contribution and has important repercussions for air quality in Santa Barbara County.

10. CONCLUSIONS

In the Santa Barbara Channel, natural marine hydrocarbon seeps offshore Coal Oil Point are principally responsible for beach tar along the coastline [Welday, 1977; Hartman and Hammond, 1981] and a significant contributor of pollution to the atmosphere [Saxena and Oliver, 1984; Killus and Moore, 1991]. This thesis examines spatial and temporal changes observed in the distribution and emission of these seeps, presents estimates of their prolific volumetric discharge, and discusses possible mechanisms which may be responsible for these observations.

In addition to the issue of local pollution, seepage may also be an important process on a global scale, introducing significant quantities of liquid petroleum [Wilson *et al*., 1974; Kvenholden and Harbaugh, 1983] and methane [Hovland *et al*., 1993] to the marine environment. Estimates of quantities associated with seepage are also important in assessing volumes of fluid flow of gaseous or liquid hydrocarbons within the earth's crust which is significant since fluids can act as markers and tracers of diagenetic processes. Fluid movement can also accompany earthquake swarms and may therefore be an important factor influencing seismic activity and structural evolution. These factors make this subject an important topic of scientific inquiry.

The results of this study show that the spatial distribution and discharge rates of the natural hydrocarbon seeps offshore Coal Oil Point are primarily governed by the offshore geologic structure. In addition, distribution and rates of seepage vary over time. An inferred long term trend of declining areal extent of seepage and reduction of seepage volumes spatially coincident with offshore oil platform Holly support the notion that drawing down of reservoir hydrocarbons through production has led to a decline in natural seepage. This effect is estimated to have reduced natural seep emissions within 13 km^2 of Holly approximately 50,000 ± 20,000 m^3/day between 1973 and 1995 with a corresponding decrease in areal cover from 0.9 to 0.4 km^2. Presumably this trend should continue into the future with ongoing production.

An estimate of current seepage for the entire Coal Oil Point offshore area (summarized in Table 2) suggests oil seepage is presently on the order of 20,000 - 30,000 liters/day and gas emission on the order of 1-2 x 10^5 m^3/day. This includes emission of methane, a greenhouse gas (2.4-5 x 10^{10} g/year), and ROG's which are precursors to smog forming ozone (20-40 metric tons/day). This confirms the notion that seepage is a significant natural source of hydrocarbons in the local environment and strengthens the case that such processes may also be important at the global scale.

APPENDIX 1: CALCULATION OF BUBBLE RISE VELOCITIES

Bubble rise velocities are calculated from [Wallis, 1974] equation (26):

$$v_\infty = \sqrt{\frac{ga\Delta\rho}{\rho_c}} \qquad \text{(A1.1)}$$

where v_∞ is the terminal bubble rise velocity, *g* is acceleration due to gravity, *a* is bubble radius, $\Delta\rho$ is the density difference between the bubbles and the surrounding (continuous) medium, and ρ_c is the density of the continuous medium. Equation (A1.1) is valid for relatively large bubbles which assume a "spherical cap" and flat base during ascent. Viscous and surface tension forces are neglected, and terminal velocity is due to the balance between form drag and buoyancy. Good experimental agreement has been observed for equation (A 1.1) for air bubbles in water. For methane bubbles in seawater, $\rho_{CH4} << \rho_{H20}$, so $\Delta\rho \approx \rho_c$ and thus $v_\infty \approx \sqrt{ga}$. For the mean radius a = 0.6 cm of the observed seep gas bubble distribution (Figure 12b), v_∞= 24 cm/sec.

APPENDIX 2: ERROR CALCULATION OF SLOPE

Error in the calibration coefficient c used in equation (8.3.1) is taken from the standard deviation in slope for a linear least squares fit given by Taylor [1982]:

$$\sigma_c^2 = N\sigma_E^2 / \Delta \qquad \text{(A2.1)}$$

where

$$\sigma_E^2 = \frac{1}{N-2}\sum_{i=1}^{N}(E_i - c(\bar{\delta}\cdot A)_i)^2 \qquad \text{(A2.2)}$$

and

$$\Delta = N(\sum(\bar{\delta}\cdot A)_i^2) - (\sum(\bar{\delta}\cdot A)_i)^2 \qquad \text{(A2.3)}$$

Additional possible sources of error not accounted for by this calculation include the following:

(1) Systematic errors in equipment including errors due to poor resolution and low dynamic range of the analog data.
(2) Errors in interpretation, such as mistaking seeps for schools of fish or kelp, which can have similar acoustic signatures.
(3) Errors arising from differences in navigational coverage.
(4) Errors due to drift of seep bubbles in the water column.
(5) Errors from unaccounted for dissolution of seep gases within the water column.
(6) Errors due to variations in gas composition from that presented in Table 1.
(7) Errors in processing such as rounding errors, filtering errors, and errors resulting from interpolation, averaging, and contouring operations.
(8) Errors related to acoustic response including:
    (a) Errors resulting from variations in bubble distribution.
    (b) Affect of different acoustic frequencies.
    (c) Variation in gas composition.
    (d) Changes in ambient pressure.
    (e) Multi-bubble reverberations.
    (f) Transmission loss of acoustic energy due to the presence of bubbles.
    (g) Effects of resonance such as failure to excite bubbles to resonance due to insufficient pulse width.

REFERENCES

Akulichev, V. A., Bulanov, V. A., and Kienin, S. A., 1986. "Acoustic sensing of gas bubbles in the ocean medium", *Soviet Phys. Acoustics*, v. 32, p. 177-180.

Allen, A. A., Schlueter, R. S., Mikolaj, P. G., 1970. "Natural Oil Seepage at Coal Oil Point, Santa Barbara, California", *Science*, v. 170, p. 974-977.

Bartsch, E. C., Gurrola, L. D., Francis, R. D., Quigley, D. C., Hornafius, J. S., and Luyendyk, B. P., 1996. "Structural Control of the Spatial Distribution of Hydrocarbon Seeps in the Northern Santa Barbara Channel, California", in *EOS Trans. Amer. Geophys. Union*, v. 77(46), p. F419.

California Division of Oil and Gas, 1991. *California Oil and Gas Fields, Volume II, Southern, Central, and Offshore California*, 3rd edition, Publication No. TR12, Sacramento.

Cicerone, R. J., and Oremland, R. S., 1988. "Biogeochemical Aspects of Atmospheric Methane", *Global Biogeochemical Cycles*, v.2(4), p. 299-327.

Clarke, R. H., and Cleverly, R. W., 1991. "Petroleum seepage and post accumulation migration", in *Petroleum Migration*, Geol. Soc. Sp. Publ. No. 59, W. A. England and A. J. Fleet, Editors, Geological Society of London, p. 265-271.

Clay, C. S., and Medwin, H., 1977. *Acoustical Oceanography*, John Wiley and Sons.

Clester, S. M., Hornafius, J. S., Scepan, J., and Estes, J. E., 1996. "Quantification of the Relationship Between Natural Gas Seepage Rates and Surface Oil Volume in the Santa Barbara Channel" in *EOS Trans. Amer. Geophys. Union*, v. 77(46), p. F420.

Cordell, R. J., 1972. "Depths of Oil Origin and Primary Migration: A review and critique", *AAPG Bull.*, v. 56(10), p. 2029-2067.

Craft, B. C. and Hawkins, M. F., 1959. *Applied Petroleum Reservoir Engineering*, Prentice-Hall, Englewood Cliffs, New Jersey, 437 p.

Cynar, F. J., and Yayanos, A., 1992. "The distribution of methane in the upper waters of the Southern California Bight", *J. Geophys. Res.*, v. 97(C7), p. 11269-11285.

Dando, P. R., and Hovland, M., 1992. "Environmental effects of submarine seeping natural gas", *Continental Shelf Research*, v. 12(10), p. 1197-1207.

Doligez, B. (ed.), 1987. *Migration of Hydrocarbons in Sedimentary Basins*, IFP Exploration Research Conference.

Du Rouchet, J., 1981. "Stress Fields, a key to oil migration", *AAPG Bull*., v. 65, p. 74-85.

England, W. A., and Fleet, A. J., 1991. *Petroleum Migration*, Geological Society Special Publication No. 59, Geological Society of London.

Eremenko, N. A., and Michailov, I. M., 1974. "Hydrodynamic Pools at Faults", *Bulletin of Canadian Petroleum Geology*, v. 22(2), p. 106-118.

Estes, J. E., Crippen, R. E., and Star, J. L., 1985. "Natural oil seep detection in the Santa Barbara Channel, California, with Shuttle Imaging Radar", *Geology*, v. 13, p. 282-284.

Field, M. E., and Jennings, A. E., 1987. "Seafloor gas seeps triggered by a northern California earthquake", *Marine Geology*, v. 77, p. 39-51.

Fischer, P. J., 1977. "Oil and tar seeps, Santa Barbara basin, California", in *California Offshore Gas, Oil, and Tar Seeps*, California State Lands Commission, Sacramento, CA, p. 1-62.

Fischer, P. J, and Stevenson, A. J., 1973. "Natural Hydrocarbon Seeps along the Northern Shelf of the Santa Barbara Basin", in *Santa Barbara Channel Revisited*, AAPG Trip 3, Annual Meeting AAPG, SEPM, SEG.

Gibbs, J. F., Healy, J. H., Raleigh, C. B., and Coakley, J., 1973. "Seismicity in the Rangely, Colorado, area: 1962-1970", *Bull. Seis. Soc. Amer*., v. 63(5), p. 1557-1570.

Guthrie, L. D., and Rowley, P. R., 1983. "Containment of Naturally Occurring Subsea Hydrocarbon Emissions - A Project Review", 15th Offshore Technology Conference, Paper 4446, p. 33-38.

Hartman, B., and Hammond, D., 1981. "The use of carbon and sulfur isotopes as correlation parameters for the source identification of beach tar in the southern California borderland", *Geochemica et Cosmochemica Acta*, v. 45, p. 309-319.

Healy, J. H., Rubey W. W., Griggs, D. T., and Raleigh, C. B., 1968. "The Denver Earthquakes", *Science*, v. 161, p. 1301-1310.

Hill, D. P., 1977. "A Model for Earthquake Swarms", *Journal of Geophysical Research*, v. 82(8), p. 1347-1352.

Hovland, M., and Judd, A. G., 1988. *Seabed Pockmarks and Seepages, Impact on Geology, Biology, and the Marine Environment*, Graham and Trotman.

Hovland, M., Judd, A. G., and Burke, R. A., 1993. "The Global Flux of Methane from Shallow Submarine Sediments", *Chemosphere*, v. 26, p. 559-578.

Hubert, M. K., and Rubey, W. W., 1959. "Role of fluid pressure in mechanics of overthrust faulting", *Bull. Geol. Soc. Amer*., v. 70, p. 115-166.

Hunt, J. M., 1979. *Petroleum Geochemistry and Geology*, W. H., Freeman Co.

Isaacs, C. M., and Peterson, N. F., 1987. "Petroleum in the Miocene Monterey Formation, California" in *Siliceous Sedimentary Rock-Hosted Ores and Petroleums,* Hem, J. R., (ed.), Van Nostrand Reinhold, New York, p. 83-116.

Judd, A. G., and Hovland, M., 1992. "The evidence of shallow gas in marine sediments", *Continental Shelf Research*, v. 12, p. 1081-1095.

Killus, J. P., and Moore, G. E., 1991. "Factor analysis of hydrocarbon species in the south central coast air basin", *Journal of Applied Meteorology*, v. 30, p. 733-743.

Kolpack, R. L., 1977. "Relationship of migration of natural seep material to oceanography of Santa Barbara Channel", in *California Offshore Gas, Oil, and Tar Seeps*, California State Lands Commission, p. 226-255.

Kraus, S. P., Estes, J. E., Atwater, S. G., Jensen, J. R., and Volimers, R. R., 1977. "Radar Detection of Surface Oil Slicks", *Photogrammetric Engr. and Remote Sensing*, v. 43(12), p. 1523-1531.

Krooss, B. M., Leythaeuser, D., and Schaefer, R. G., 1992. "The Quantification of Diffusive Hydrocarbon Losses Through Cap Rocks of Natural Gas Reservoirs - A Reevaluation", *AAPG Bull*., v. 76(3), p. 403-406.

Kvenholden, K. A., 1993. "Gas Hydrates - Geological Perspective and Global Change", *Reviews of Geophysics*, v. 31(2), p.173-187.

Kvenholden, K. A., and Harbaugh, J. W., 1983. "Reassessment of the rates at which oil from natural sources enters the marine environment", *Marine Environmental Research*, v. 10, p. 223-243.

Lacroix, A.V., 1993, Unaccounted-for sources of fossil and isotopically-enriched methane and their contribution to the emissions inventory: A review and synthesis, *Chemosphere*, v. 26, p. 507-557.

Landes, K. K., 1973. "Mother Nature as an Oil Polluter", *AAPG Bull*., v. 57(4), p. 637-641.

Lange, N. A., Forker, G. M., Burington, R. S., 1941. *Handbook of Chemistry*, Handbook Publishers, Inc., Sandusky, Ohio.

Leythauser, D., Schaefer, R. G., and Yukler, A., 1982. "Role of diffusion in primary migration of hydrocarbons", *AAPG Bull*., v. 66(4), p. 408-429.

Link, W. K., 1952. "Significance of Oil and Gas Seeps in World Oil Exploration", *AAPG Bull*., 6(8), p. 1505-1540.

MacDonald, G. J., 1990. "Role of Methane Clathrates in Past and Future Climates", *Climate Change*, v. 16, p. 247-281.

Machel, H.G., and Burton, E. A., 1991. "Causes and Spatial Distribution of Anomalous Magnetization in Hydrocarbon Seepage Environments", *AAPG Bull*., v. 75(12), p. 1864-1876.

McAuliffe, C. D., 1979. "Oil and Gas Migration - Chemical and Physical Constraints", *AAPG Bull*., v. 63(5), p.761-781.

Medwin, H., 1977a. "Counting bubbles acoustically: a review", *Ultrasonics*, p. 7-13.

Medwin, H., 1977b. "Acoustical determinations of bubble-size spectra", *Journal of the Acoustical Society of America*, v. 62 (4), p. 1041-1044.

Mikolaj, P. G., and Ampaya, J. P., 1973. "Tidal Effects on the Activity of Natural Submarine Oil Seeps", *Marine Technical Society Journal*, v. 7, p. 25-28.

Nisbet, E. G., 1990. "The end of the ice age", *Canadian Journal of Earth Science*, v. 27, p. 148-157.

Price, L. C., 1976. "Aqueous Solubility of Petroleum as Applied to its Origin and Primary Migration", *AAPG Bull*., v. 60(2), p. 2 13-244.

Price, L. C., 1979. "Aqueous Solubility of Methane at Elevated Pressures and Temperatures", *AAPG Bull*., p. 1527-1533.

Reed, W. E., and Kaplan, I. R., 1977. "The Chemistry of Marine Petroleum Seeps", *Journal of Geochemical Exploration*, v. 7, p. 255-293.

Rintoul, B., 1982. "ARCO Caps Santa Barbara Channel Seep", *Pacific Oil World*, 74(11), p. 6-9.

Roberts, W. H., and Cordell, R. J., 1980. *Problems of Petroleum Migration,* AAPG Studies in Geology No. 10.

Santa Barbara Air Pollution Control District, 1994. "The 1994 Clean Air Plan", Appendix D., Table 3.2, Santa Barbara, CA.

Saxena, P., and Oliver, W. R., 1984. "Estimation of reactive organic gas emissions from offshore oil and gas seeps in the Santa Barbara Channel", Systems Applications, Inc., report SYSAPP-84/197, prepared for the U. S. Environmental Protection Agency, San Francisco, CA, 25 pp.

Shine, K. P., Derwent, R. G., Wuebbles, D. J., and Morcrette, J. J., 1990. "Radiative forcing of climate", in *Climate Change, the IPCC Scientific Assessment*, edited by J. T. Houghton, G. J. Jenkins, and J. J. Ephraums, p. 41-68, Cambridge University Press, New York.

Sibson, R. H., 1996. "Structural Permeability of fluid-driven fault-fracture meshes", *Journal of Structural Geology*, v. 18(8), p. 1031-1042.

Smith, W. and Wessel, P., 1990. "Gridding with continuous curvature splines in tension", *Geophysics*, v. 55, p. 293-305.

Straughan, D. and Abbott, B. C., 1972. "The Santa Barbara oil spill: ecological changes and natural oil leaks", In: *Water pollution by oil* (Hepple, P. (Ed.)), Institute of Petroleum, London, p. 257-262.

Sweet, W. E., 1973. "Marine Acoustical Hydrocarbon Detection", 5th Offshore Technology Conference, Paper 1803.

Sylvester, A. G., Smith, S. W., and Scholz, C. H., 1970. "Earthquake swarm in the Santa Barbara Channel, California, 1968", *Bull. Seismological Society of America*, v. 60(4), p. 1047-1060.

Taylor, J. R., 1982. *An Introduction to Error Analysis, The Study of Uncertainties in Physical Measurements*, University Science Books, Oxford University Press.

Tedesco, S. A., 1995. *Surface Geochemistry in Petroleum Exploration*, Chapman and Hall.

Tinkle, A. R., Antoine, J. W., and Kuzela, R., 1973. "Detecting natural gas seeps at sea", *Ocean Industry*, v. 8, p. 139-142.

Tissot, B., 1987. "Migration of Hydrocarbons in Sedimentary Basins: A Geological, Geochemical, and Historical Perspective", in *Migration of Hydrocarbons in Sedimentary Basins*, edited by B. Doligez, 2nd IFP Exploration Research Conference, p. 1-19.

Urick, R. J., 1983. *Principles of Underwater Sound*, Mcgraw-Hill, 3rd Edition.

Vagle, S., and Farmer, D. M., 1992. "The measurement of bubble-size distributions by acoustical backscatter", *Journal of Atmospheric and Oceanic Technology*., v. 9, p. 630-644.

Vernon, J. W., and Slater, R. A., 1963. "Submarine tar mounds, Santa Barbara County, California", *AAPG Bull*., v. 47, p. 1624-1627.

Wallis, G. B., 1974. "The Terminal Speed of Single Drops or Bubbles in an Infinite Medium", *International Journal of Multiphase Flow*, v. 1, p. 491-511.

Watson, R. T., Rodhe, H., Oeschger, H., and Siegenthaler, U., 1990. "Greenhouse gases and aerosols", in *Climate Change, the IPCC Scientific Assessment*, edited by J. T. Houghton, 0. J. Jenkins, and J. J. Ephraums, p. 4 1-68, Cambridge University Press, New York.

Welday, E. E., 1977. "Oil and Tar on Santa Barbara region beaches", in *California Offshore Gas, Oil, and Tar Seeps*, California State Lands Commission, Sacramento, CA, p. 347-371.

Wilkinson, E. R., 1972. "California Offshore Oil and Gas Seeps", California Division of Oil and Gas, Pubi. No. TRO8, 11 p.

Wilson, R. D., Monaghan P. H., Osanik, A., Price, L. C., and Rogers, M. A., 1974. "Natural Marine Oil Seepage", *Science*, v. 184, p. 857-864.

Wu, J., 1981. "Bubble Populations and Spectra in Near Surface Ocean: Summary and Review of Field Measurements", *J. of Geophys. Res*., v. 86(C1), p. 457-463.

ACKNOWLEDGEMENTS

This work was supported by funding from
the University of California Energy Institute
Grant #08960643
and
the Mineral Management Service
Grant # 13093

The author would like to express his appreciation to

Dr. J. Scott Hornafius, Mobil Oil Corporation, Professor Bruce Luyendyk, Professor James Boles, Professor Jordan Clark, Professor Libe Washburn, Professor Robert Francis, Professor Rachel Haymon, Erik Bartsch, Fred Sanford, Gordon Cota, Gretchen Mullendore, David Salazar, Priscilla D'Aquino, and the Seawatch crew

for invaluable assistance in the completion of this work.

The Department of the Interior Mission

As the Nation's principal conservation agency, the Department of the Interior has responsibility for most of our nationally owned public lands and natural resources. This includes fostering sound use of our land and water resources; protecting our fish, wildlife, and biological diversity; preserving the environmental and cultural values of our national parks and historical places; and providing for the enjoyment of life through outdoor recreation. The Department assesses our energy and mineral resources and works to ensure that their development is in the best interests of all our people by encouraging stewardship and citizen participation in their care. The Department also has a major responsibility for American Indian reservation communities and for people who live in island territories under U.S. administration.

The Minerals Management Service Mission

As a bureau of the Department of the Interior, the Minerals Management Service's (MMS) primary responsibilities are to manage the mineral resources located on the Nation's Outer Continental Shelf (OCS), collect revenue from the Federal OCS and onshore Federal and Indian lands, and distribute those revenues.

Moreover, in working to meet its responsibilities, the **Offshore Minerals Management Program** administers the OCS competitive leasing program and oversees the safe and environmentally sound exploration and production of our Nation's offshore natural gas, oil and other mineral resources. The MMS **Royalty Management Program** meets its responsibilities by ensuring the efficient, timely and accurate collection and disbursement of revenue from mineral leasing and production due to Indian tribes and allottees, States and the U.S. Treasury.

The MMS strives to fulfill its responsibilities through the general guiding principles of: (1) being responsive to the public's concerns and interests by maintaining a dialogue with all potentially affected parties and (2) carrying out its programs with an emphasis on working to enhance the quality of life for all Americans by lending MMS assistance and expertise to economic development and environmental protection.